Electronic Supporting Information (ESI) to:

Oxochlorin frameworks confining a β-hydroxyketone moiety

Nivedita Chaudhri[*,a,b] Matthew J. Guberman-Pfeffer[c], Matthias Zeller[d],*

and Christian Brückner[a,]*

[a] *Department of Chemistry University of Connecticut, Unit 3060, Storrs, CT 06269-3060, U.S.A.*

[b] *Department of Chemistry, Guru Nanak Dev University Amritsar, Punjab-143005, India*

[c] *Department of Chemistry and Biochemistry, Baylor University, One Bear Place #97348, Waco, Texas 76706, United States*

[d] *Department of Chemistry Purdue University, 560 Oval Drive, West Lafayette, IN 47907-2084, U.S.A.*

* Corresponding authors: nivi.chaudhri@gmail.com (N.C.) and c.bruckner@uconn.edu(C.B.)

ESI Table of Contents

Experimental Section

Materials: Solvents and reagents were used as received. Aluminum-backed, silica gel 60, 250 μm thickness analytical plates, 20 × 20 cm, glass-backed, silica gel 60, 500 μm thickness preparative TLC plates, and standard grade, 60 Å, 32-63 μm flash column silica gel were used for purifications.

Instrumentations: ^{1}H NMR and ^{13}C NMR spectra were recorded using a Bruker AVANCE II 400 MHz spectrometer. IR spectra were recorded from neat material on a Bruker Alpha FTIR spectrometer using an attenuated total reflection (ATR) diamond crystal. Low- and high-resolution mass spectra were recorded using AB Sciex API 2000 Triple Quadrupole and AB Sciex QStar Elite Quadrupole-TOF MS instruments, respectively in CH_3CN. UV-Vis data were obtained on Varian Cary 100 or Cary 50 spectrophotometers in CH_2Cl_2. The fluorescence spectra were recorded on a Cary Eclipse fluorimeter. Details of the X-ray diffractometry studies are provided below.

5-Hydroxy-7-oxo-octaethylchlorin (9): Prepared as greenish-purple powder as described in the literature;[1] data included for comparison. MW = 566.790 g/mol. R_f = 0.47 (silica/CH_2Cl_2-Hexanes, (2:1 v/v). ^{1}H NMR (400 MHz, $CDCl_3$): 13.57 (s, 1H, -OH), 9.46 (1H, *meso*-H), 9.06 (1H, *meso*-H), 8.50 (1H, *meso*-H), 3.99 (q, $_3J^{H,H}$ = 7.4 Hz, 2H, -CH_2), 3.90 (q, $_3J^{H,H}$ = 7.6 Hz, 2H, -CH_2), 3.85 - 3.66 (m, 8H, -CH_2), 2.70 – 2.61 (m, 4H, -CH_2), 1.81 - 1.68 (m, 18H, -CH_3), 0.39 (t, $_3J^{H,H}$ = 7.5 Hz, 6H, -CH_3), -0.70 (s, 2H, -NH) ppm. ^{13}C{^{1}H} NMR (101 MHz, $CDCl_3$): 214.3, 161.3, 158.0, 150.9, 145.8, 144.5, 142.6, 139.9, 139.4, 139.3, 138.8, 137.8, 137.6, 132.4, 131.3, 126.0, 101.7, 93.8, 90.4, 62.7, 30.8, 21.0, 19.6, 19.5, 19.3, 19.0, 18.5, 18.4, 18.0, 17.8, 17.7, 16.9, 8.3 ppm. UV-vis (CH_2Cl_2) λ_{max} (log ε): 337 (4.22), 403 (4.79), 421 (4.95), 510 (3.46), 551 (3.64), 584 (3.90), 641 (4.00). Fluorescence (CH_2Cl_2, $\lambda_{excitation}$ = 421 nm) $\lambda_{max\text{-}emission}$ = 645, 703 nm. IR (diamond ATR, neat): 1645 ($\nu_{C=O}$), 3324 ($\nu_{N\text{-}H}$) cm^{-1}. HR-MS (ESI+, 100% CH_3CN, TOF): calc'd for $C_{36}H_{47}N_4O_2^+$ $[M+H]^+$ 567.3694, found 567.3668.

(1) Li, R.; Meehan, E.; Zeller, M.; Brückner, C. Surprising outcomes of classic ring-expansion conditions applied to octaethyloxochlorin, 2. Beckmann-rearrangement conditions. *Eur. J. Org. Chem.* **2017,** 1826-1834.

Reproduction of Spectra

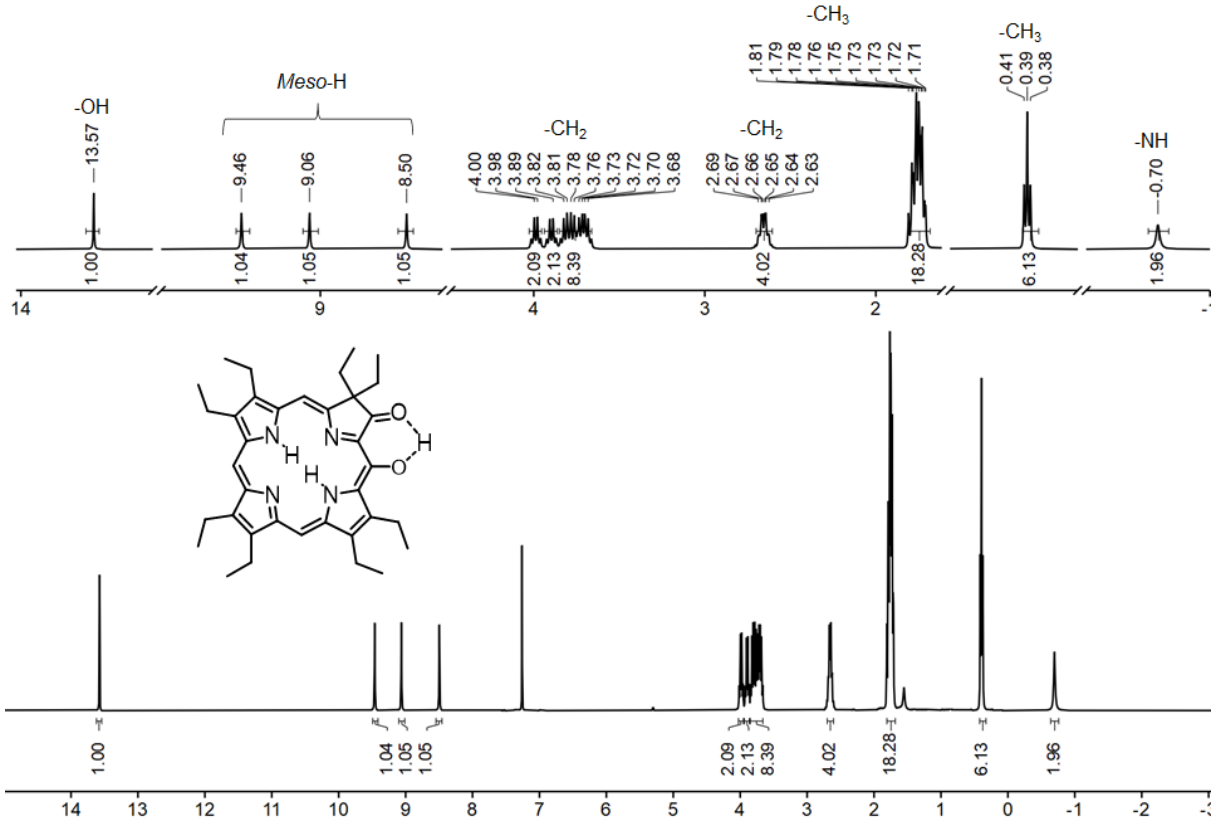

Figure S1. ^{1}H NMR spectrum (400 MHz, $CDCl_3$ at 25 °C) of 5-OH-7-oxochlorin (**9**).

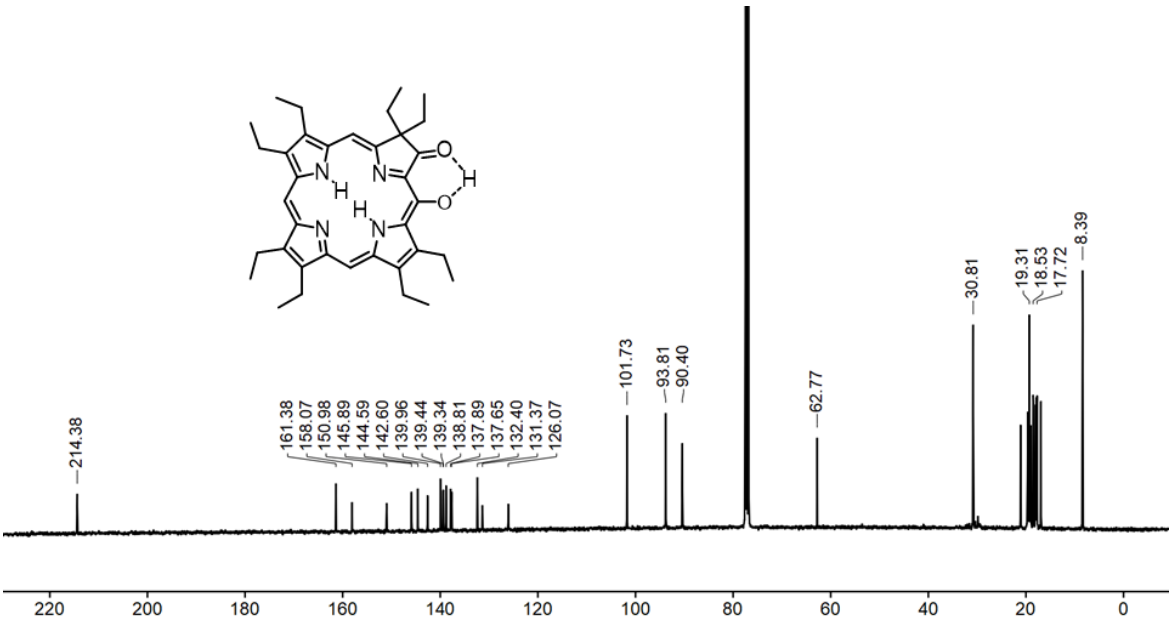

Figure S2. ^{13}C NMR spectrum (101 MHz, $CDCl_3$ at 25 °C) of 5-OH-7-oxochlorin (**9**).

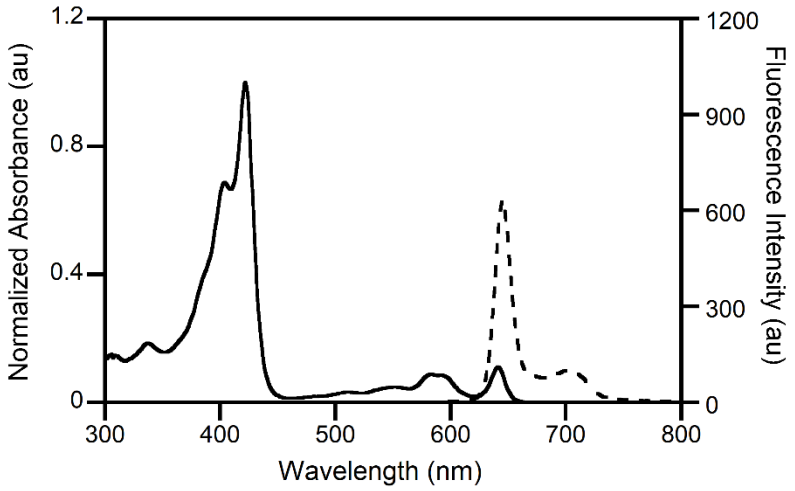

Figure S3. UV-vis (CH_2Cl_2) absorption (solid line) and fluorescence emission (CH_2Cl_2) spectra (broken line) of 5-OH-7-oxochlorin (**9**).

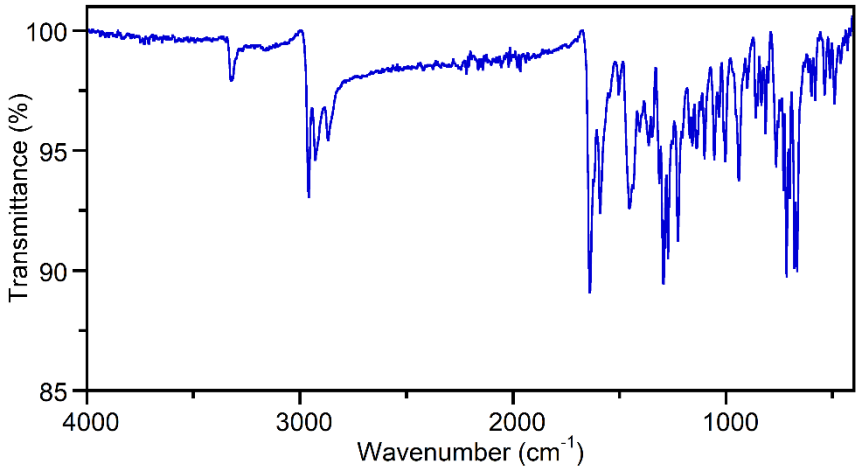

Figure S4. FT-IR Spectrum (neat, diamond ATR) of 5-OH-7-oxochlorin (**9**).

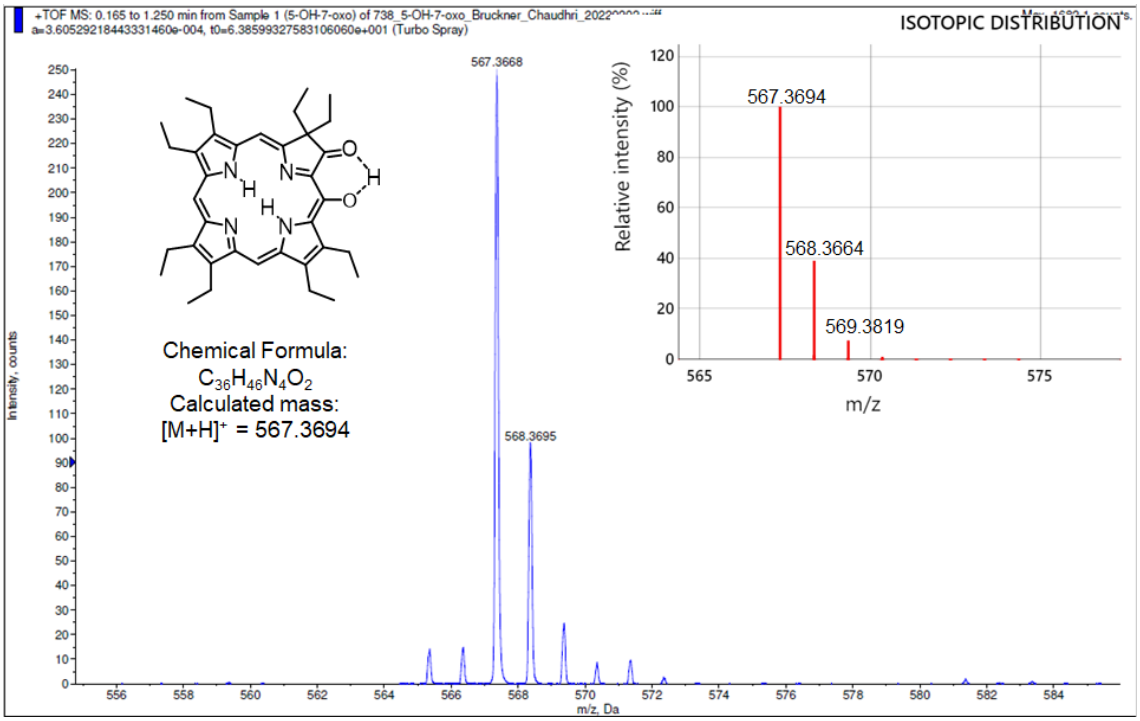

Figure S5. HR-MS Spectrum (ESI+, 100% CH_3CN, TOF) of 5-OH-7-oxochlorin (**9**).

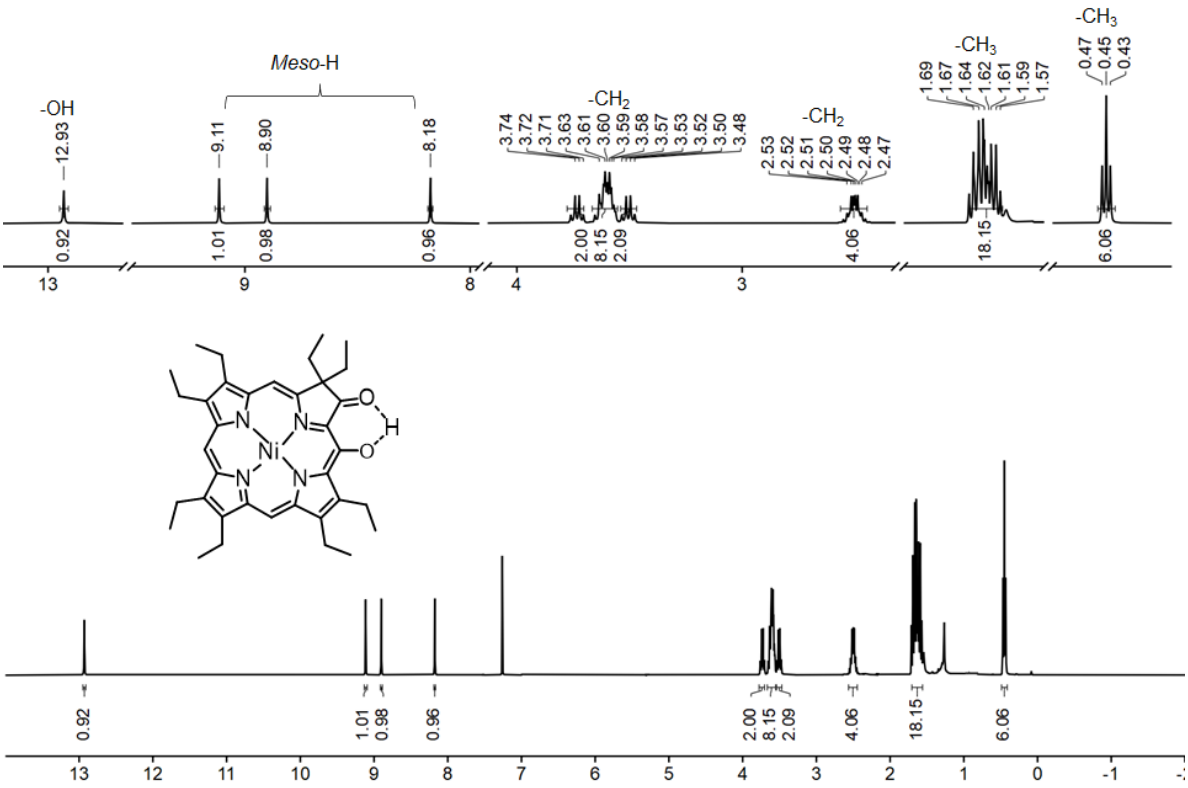

Figure S6. ^{1}H NMR spectrum (400 MHz, $CDCl_3$ at 25 °C) of 5-OH-7-oxochlorinato nickel(II) (**9Ni**).

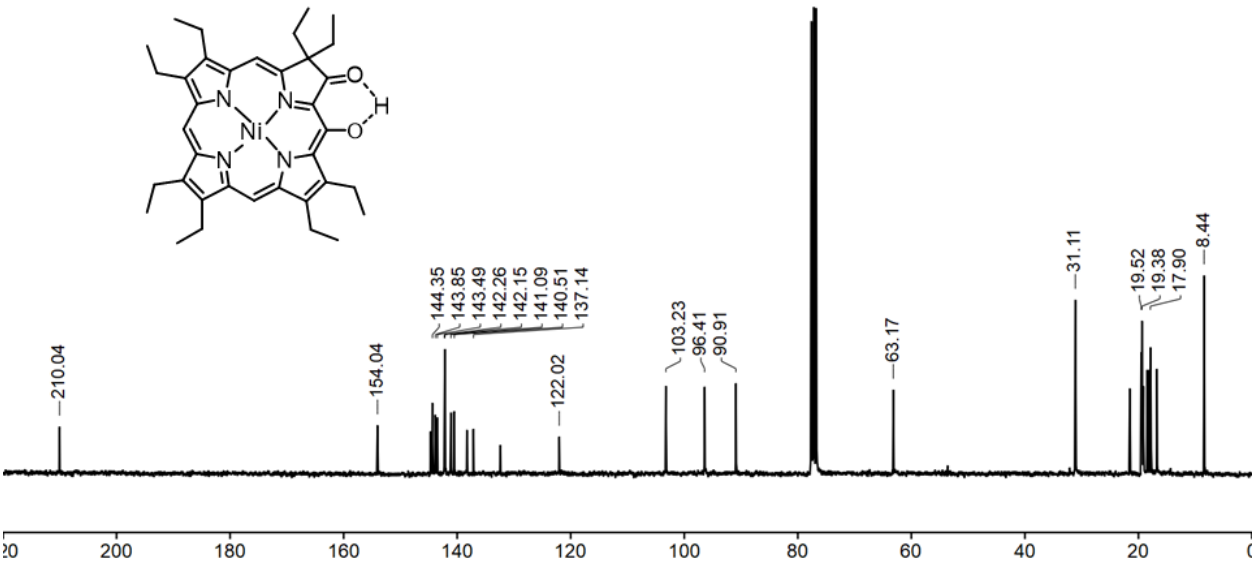

Figure S7. ^{13}C NMR spectrum (101 MHz, $CDCl_3$ at 25 °C) of 5-OH-7-oxochlorinato nickel(II) (**9Ni**).

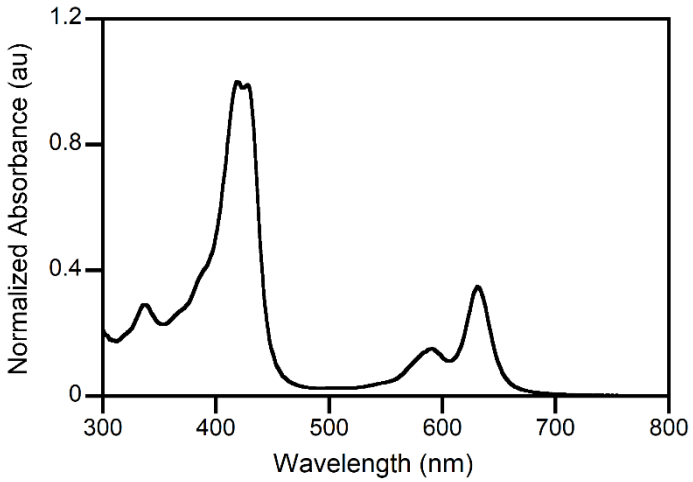

Figure S8. Normalized UV-vis (CH_2Cl_2) absorption spectrum of 5-OH-7-oxochlorinato nickel(II) (**9Ni**).

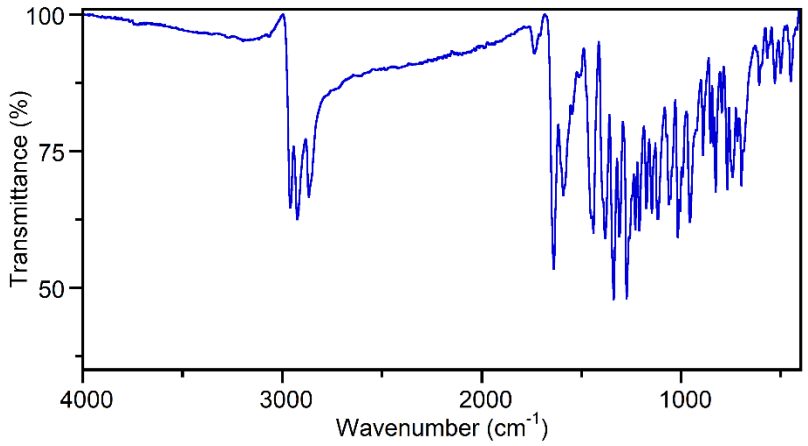

Figure S9. FT-IR Spectrum (neat, diamond ATR) of 5-OH-7-oxochlorinato nickel(II) (**9Ni**).

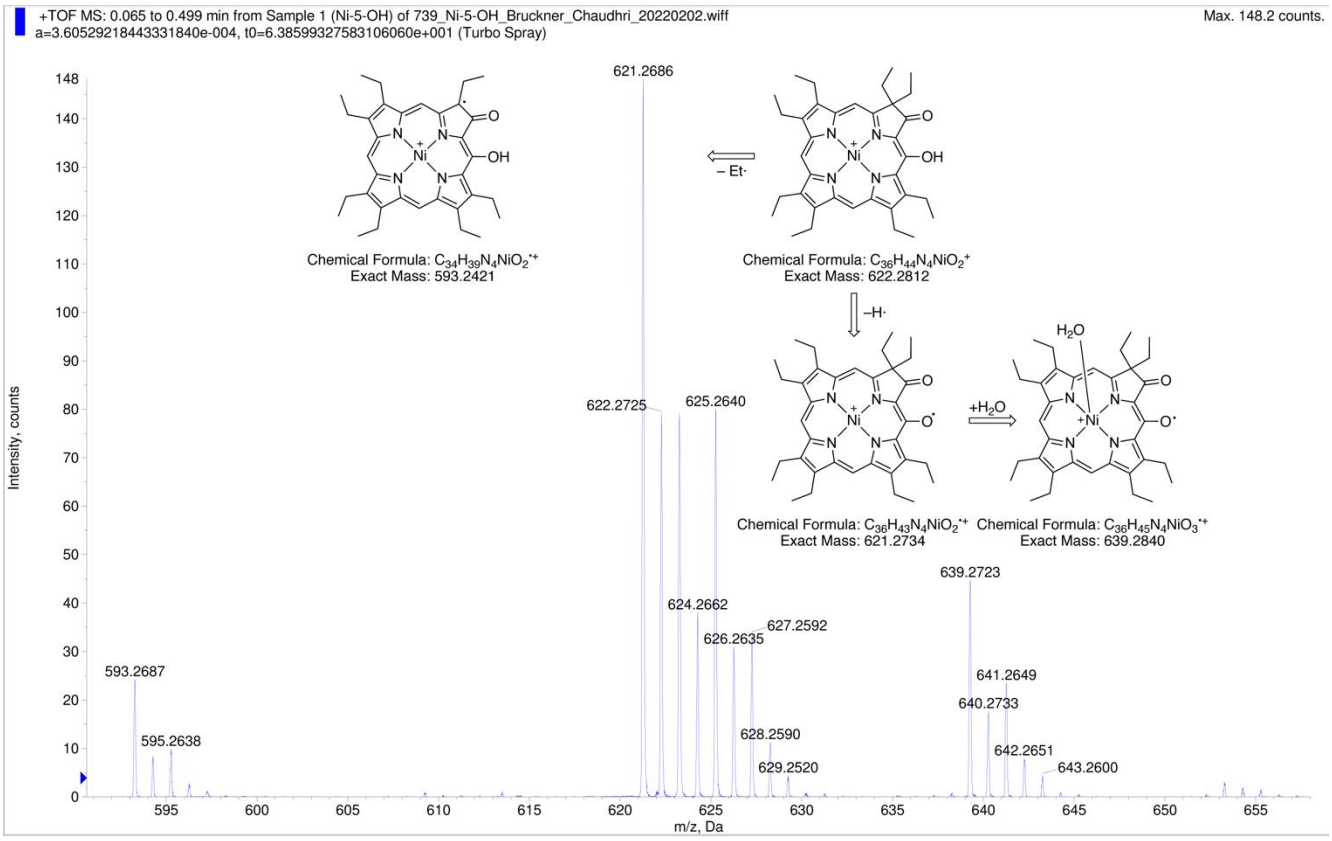

Figure S10. HR-MS Spectrum (ESI+, 100% CH_3CN, TOF) of 5-OH-7-oxochlorinato nickel(II) (**9Ni**) with its proposed reactions in the spectrometer, giving rise to the four major peak clusters observed (each matching in their isotope patterns with the calculated patterns, not shown).

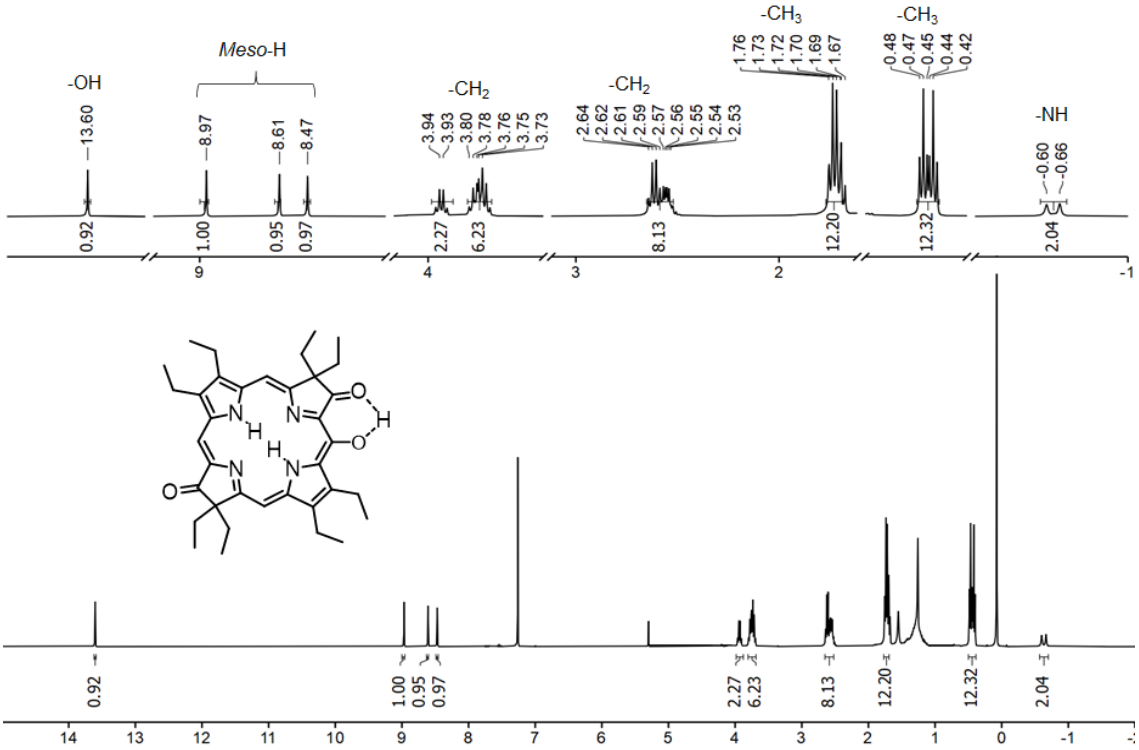

Figure S11. ^{1}H NMR spectrum (400 MHz, $CDCl_3$ at 25 °C) of 5-OH-7,17-dioxobacteriochlorin (**10**).

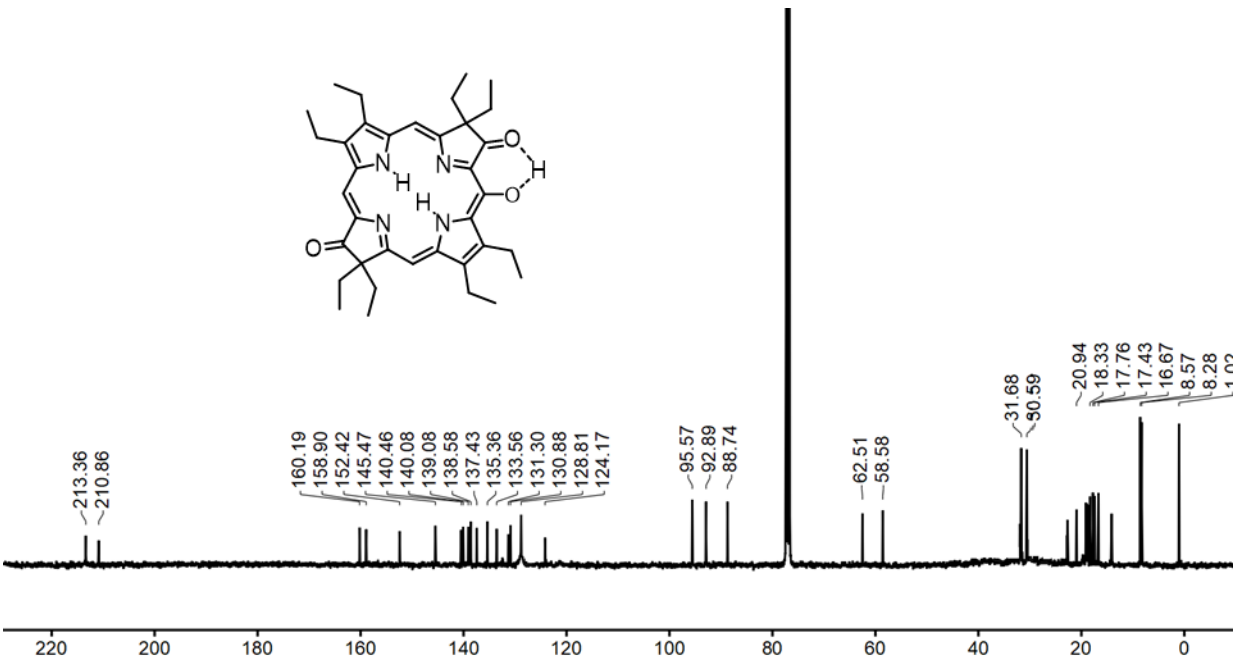

Figure S12. ^{13}C NMR spectrum (101 MHz, $CDCl_3$ at 25 °C) of 5-OH-7,17-dioxobacteriochlorin (**10**).

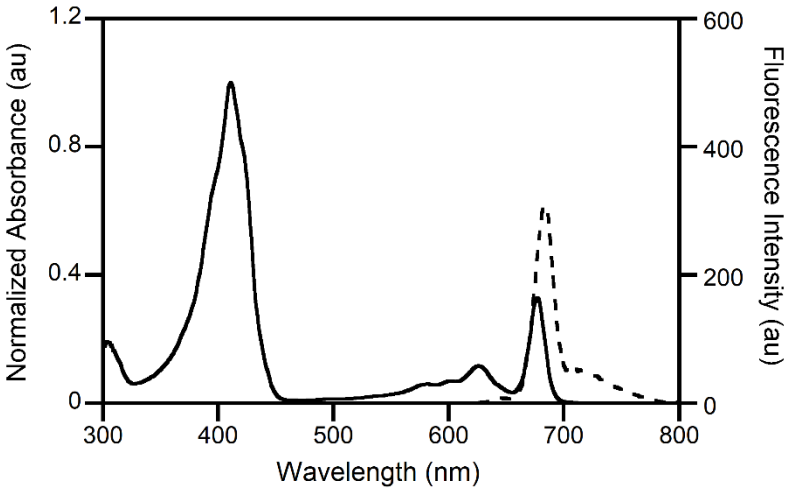

Figure S13. Normalized UV-vis (CH_2Cl_2) absorption (solid line) and fluorescence emission (CH_2Cl_2) spectra (broken line) of 5-OH-7,17-dioxobacteriochlorin (**10**).

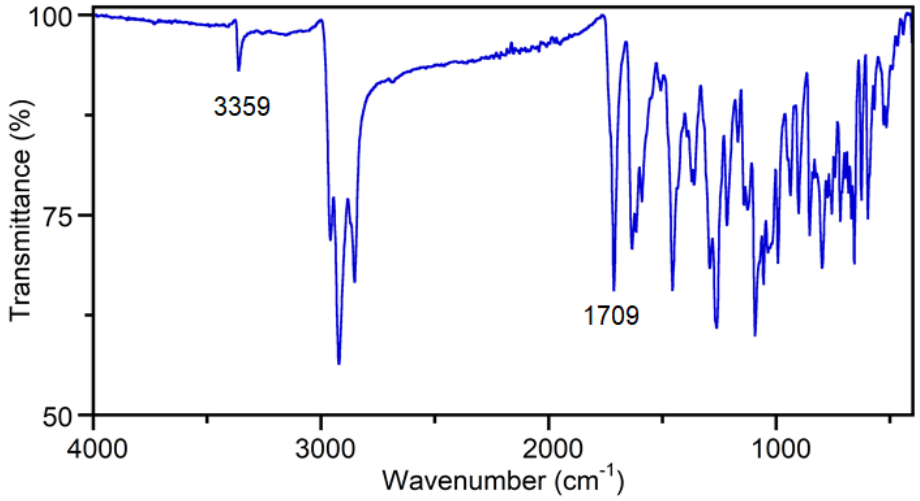

Figure S14. FT-IR Spectrum (neat, diamond ATR) of 5-OH-7,17-dioxobacteriochlorin (**10**).

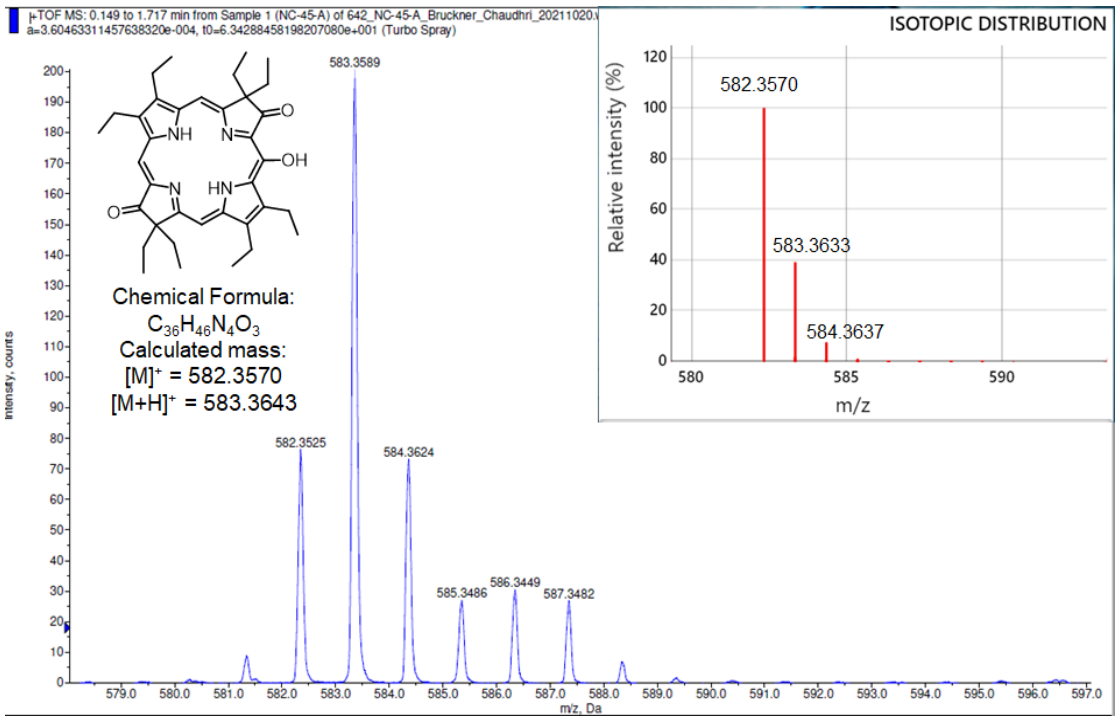

Figure S15. HR-MS Spectrum (ESI+, 100% CH_3CN, TOF) of 5-OH-7,17-dioxobacteriochlorin (**10**). Overlapping $[M]^+$ and $[M+H]^+$ peaks.

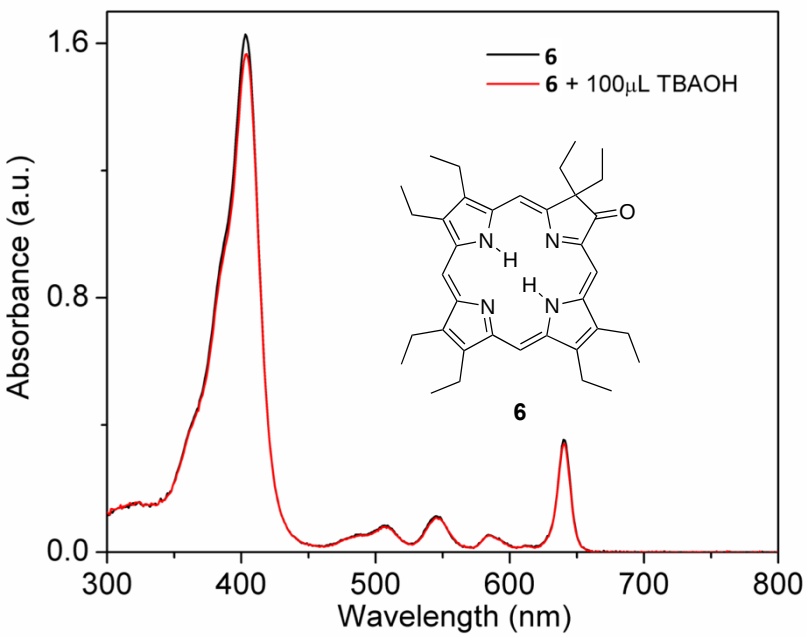

Figure S16. UV-vis spectrophotometric titration of oxochlorin **6** with TBAOH in the range indicated. Data from ref. 2, included for comparison.

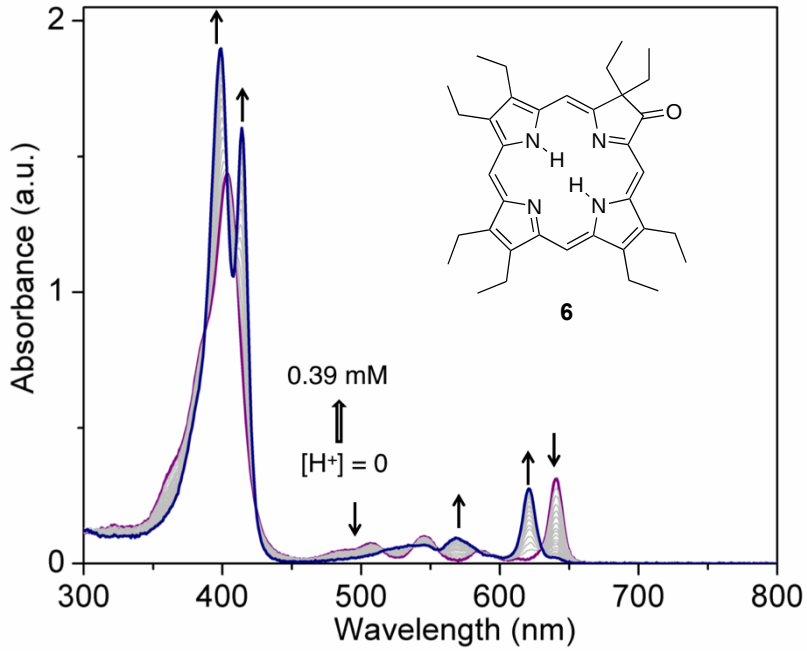

Figure S17. UV-vis spectrophotometric titration of oxochlorin **6** with TFA in the range indicated. Data from ref. 2, included for comparison.

2. D. Schnable, N. Chaudhri, R. Li, M. Zeller and C. Brückner, Evaluation of Octaethyl-7,17-dioxobacteriochlorin as a Ligand for Transition Metals *Inorg. Chem.*, 2020, **59**, 2870–2880.

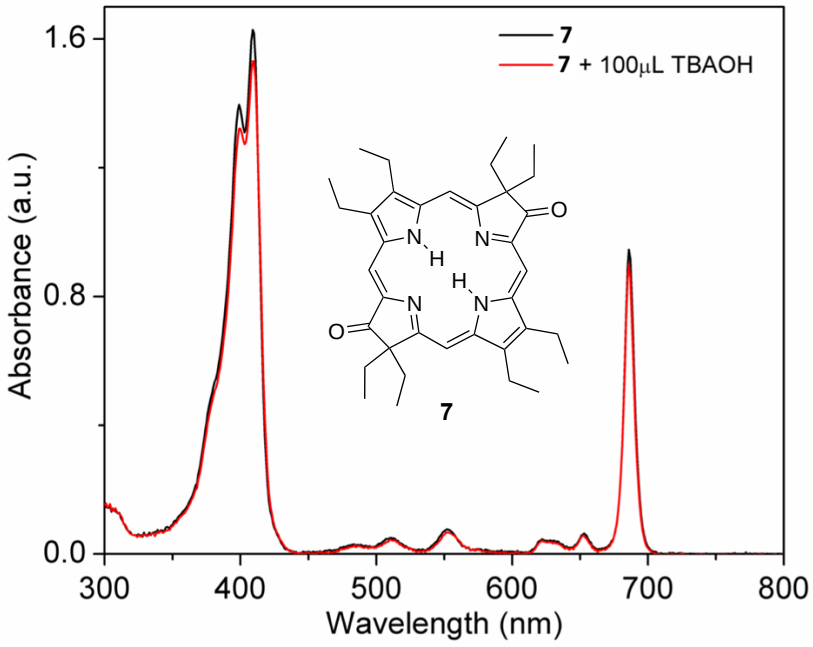

Figure S18. UV-vis spectrophotometric titration of dioxobacteriochlorin **7** with TBAOH in the range indicated. Data from ref. 2, included for comparison.

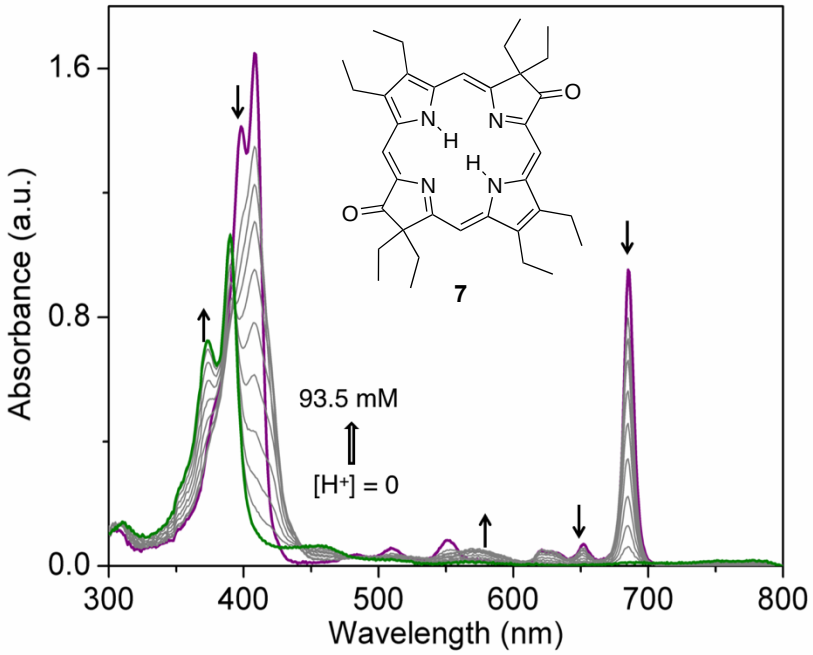

Figure S19. UV-vis spectrophotometric titration of dioxobacteriochlorin **7** with TFA in the range indicated. Data from ref. 2, included for comparison.

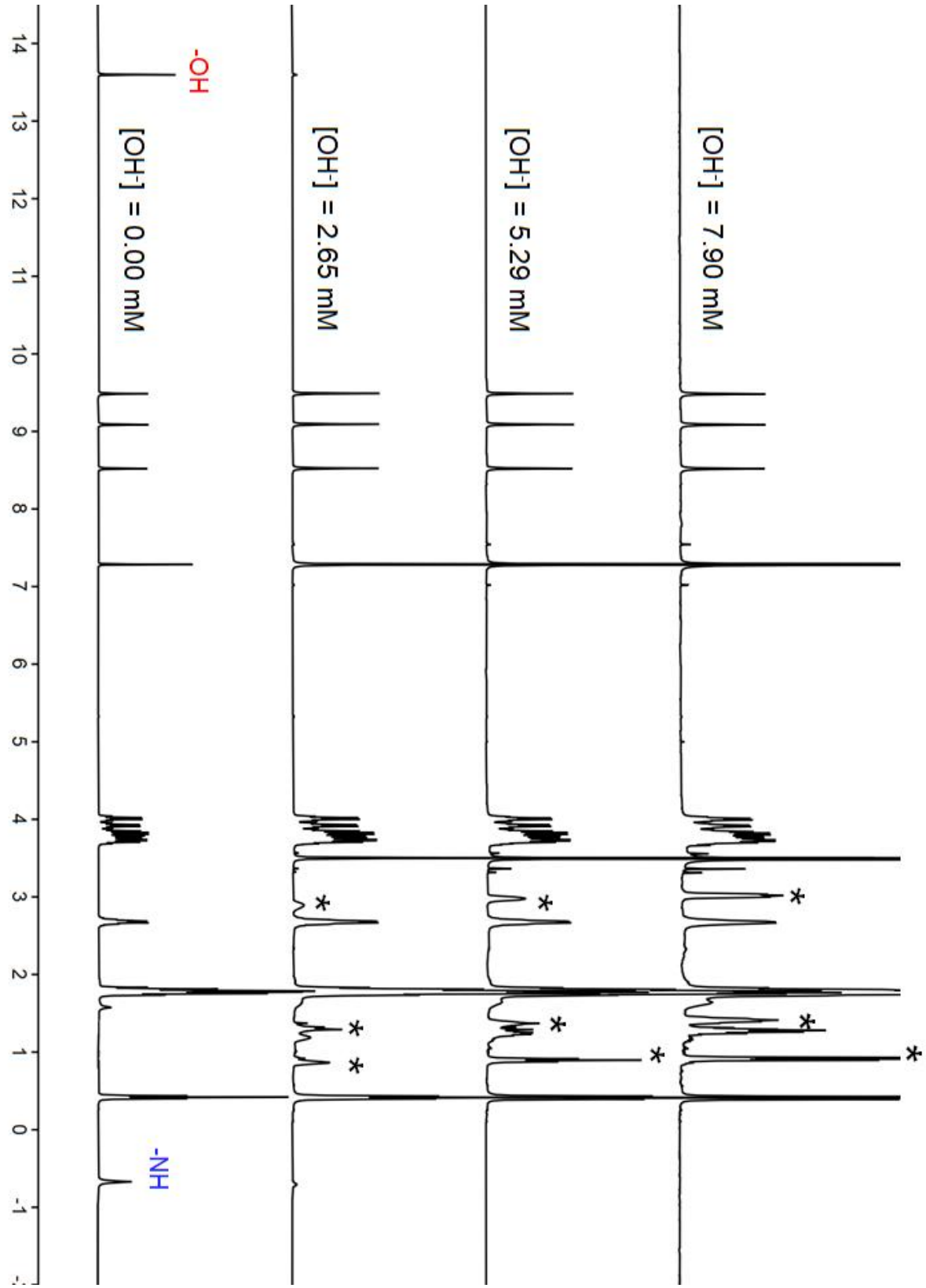

Figure S20. ^{1}H NMR spectroscopic titration (400 MHz, $CDCl_3$) of *meso*-hydroxyoxochlorin **9** (10.2 mM) with TBAOH (0.66 M in $CDCl_3$). *Indicates the signals arising from TBAOH.

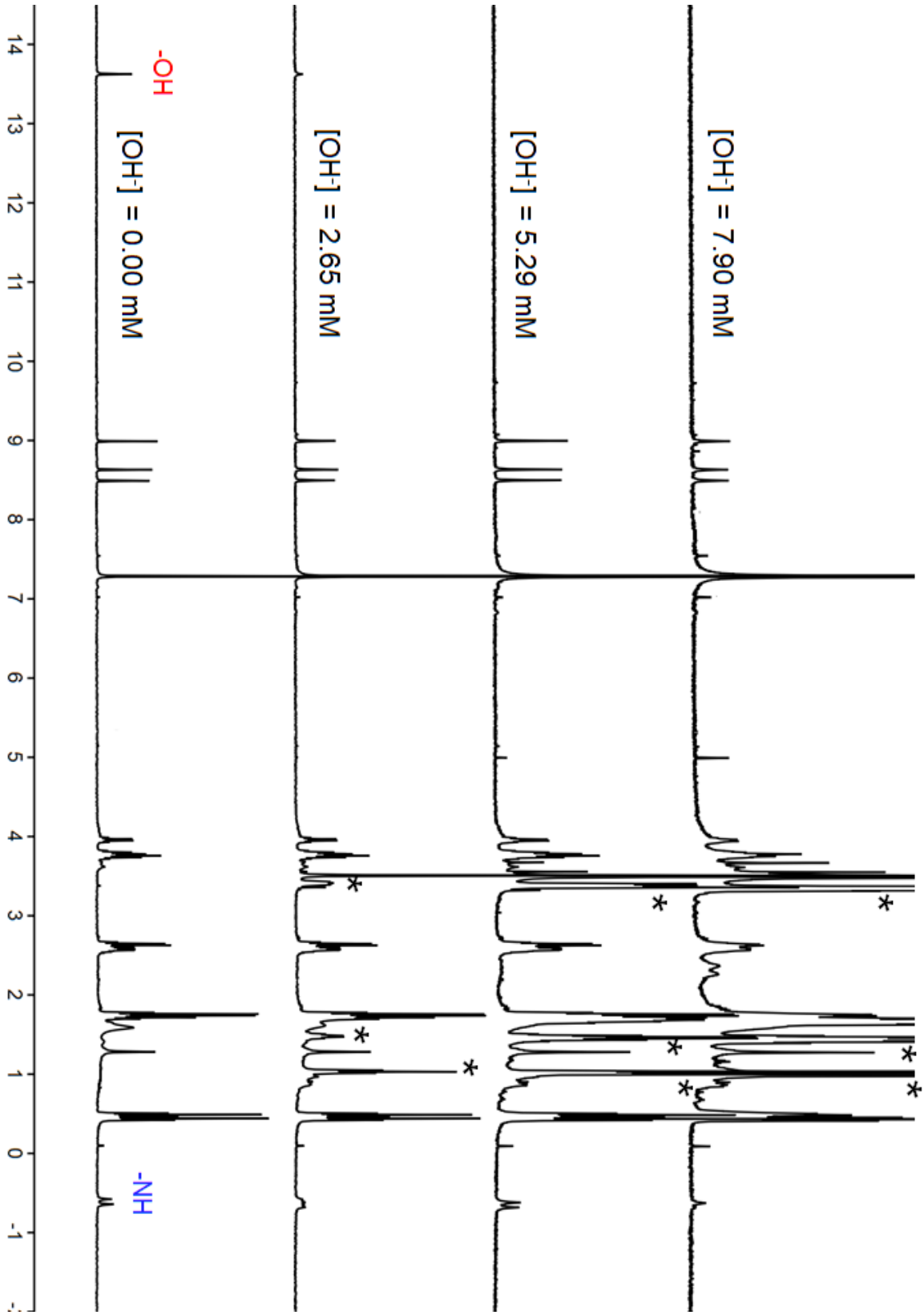

Figure S21. ^{1}H NMR spectroscopic titration (400 MHz, $CDCl_3$) of *meso*-hydroxydioxobacteriochlorin **10** (9.5 mM) with TBAOH (0.66 M in $CDCl_3$). * Indicates the signals arising from TBAOH.

Details to the computational studies

Computational Methods

All structures were optimized with the Becke, three-parameter, Lee-Yang-Parr (B3LYP) approximate density functional[31, 2] and the Pople 6-31+G(d,p) basis set.[43-6] The absence of negative frequencies in a harmonic vibrational analysis confirmed that a local minimum had been found on the potential energy surface for each molecule.

Relaxed potential energy surface scans for the rotation of the 5-OH moiety, as well as for interconversion between the 7-OXO-5-OH and 7-OH-5-OXO tautomers were performed with the same functional and basis set combination. The scans were incremented by 10° and 0.02 Å, respectively.

UV-vis spectra were simulated using time-dependent density functional theory (TD-DFT) with the same functional and basis set as for the geometry optimizations. The lowest-lying 20 singlet excited states were computed. NMR magnetic shielding tensors were computed using the gauge-including-atomic-orbitals (GIAO) method,[5] the BHandHLYP approximate density functional,[6] and the Ahlrichs

3. (a) Beck, A. D. Density-functional thermochemistry. III. The role of exact exchange. *J. Chem. Phys.* **1993**, *98*, 5648–5646. (b) Stephens, P. J.; Devlin, F. J.; Chabalowski, C. F.; Frisch, M. J. Ab initio calculation of vibrational absorption and circular dichroism spectra using density functional force fields. *J. Phys. Chem.* **1994**, *98*, 11623–11627.

4. (a) Ditchfield, R.; Hehre, W. J.; Pople, J. A. Self-consistent molecular-orbital methods. IX. An extended Gaussian-type basis for molecular-orbital studies of organic molecules. *J. Chem. Phys.* **1971**, *54*, 724–728. (b) Hehre, W. J.; Ditchfield, R.; Pople, J. A. Self—consistent molecular orbital methods. XII. Further extensions of Gaussian—type basis sets for use in molecular orbital studies of organic molecules. *The J. Chem. Phys.* **1972**, *56*, 2257–2261. (c) Hariharan, P. C.; Pople, J. A. The influence of polarization functions on molecular orbital hydrogenation energies. *Theor. Chim. Acta* **1973**, *28*, 213–222. (d) Clark, T.; Chandrasekhar, J.; Spitznagel, G. W.; Schleyer, P. V. R. Efficient diffuse function-augmented basis sets for anion calculations. III. The 3-21+ G basis set for first-row elements, Li–F. *J. Comp. Chem.* **1983**, *4*, 294–301.

5. (a) London, F. Quantum theory of interatomic currents in aromatic compounds. *J. Phys. Radium* **1937**, *8*, 397–409. (b) Reid Jr, R. V. Nuclear magnetic shielding in the hydrogen molecule. *Phys. Rev. A* **1975**, *11*, 403. (c) Ditchfield, R. Self-consistent perturbation theory of diamagnetism. I. A gage-invariant LCAO (linear combination of atomic orbitals) method for NMR chemical shifts. *Mol. Phys* **1974**, *27*, 789–807. (d) Wolinski, K.; Hinton, J. F.; Pulay, P. Efficient implementation of the gauge-independent atomic orbital method for NMR chemical shift calculations. *J. Am. Chem. Soc.* **1990**, *112*, 8251–8260.

def2-TZVP basis set.[7] This level of theory for NMR spectral simulations was previously benchmarked and recommended for porphyrinoids.[8]

All geometry and response-property calculations were performed with an ultrafine integration grid and tight self-consistent-field (SCF) convergence criteria as implemented in Gaussian 16, Revision A.03.[9]

---

6. Becke, A. D. A new mixing of Hartree–Fock and local density-functional theories. *J. Chem. Phys.* **1993**, *98*, 1372–1377.

7. Weigend, F.; Ahlrichs, R. Balanced basis sets of split valence, triple zeta valence and quadruple zeta valence quality for H to Rn: Design and assessment of accuracy. *Phys. Chem. Chem. Phys.* **2005**, *7*, 3297–3305.

8. Hewage, N.; Guberman-Pfeffer, M. J.; Chaudhri, N.; Zeller, M.; Gascón, J. A.; Brückner, C. Syntheses and Aromaticity Parameters of Hexahydroxypyrrocorphin, Porphotrilactones, and Their Oxidation State Intermediates. *J. Org. Chem.* **2022**, *87*, 12096–12108.

9. Frisch, M. J.; Trucks, G. W.; Schlegel, H. B.; Scuseria, G. E.; Robb, M. A.; Cheeseman, J. R.; Scalmani, G.; Barone, V.; Petersson, G. A.; Nakatsuji, H.; Li, X.; Caricato, M.; Marenich, A. V.; Bloino, J.; Janesko, B. G.; Gomperts, R.; Mennucci, B.; Hratchian, H. P.; Ortiz, J. V.; Izmaylov, A. F.; Sonnenberg, J. L.; Williams; Ding, F.; Lipparini, F.; Egidi, F.; Goings, J.; Peng, B.; Petrone, A.; Henderson, T.; Ranasinghe, D.; Zakrzewski, V. G.; Gao, J.; Rega, N.; Zheng, G.; Liang, W.; Hada, M.; Ehara, M.; Toyota, K.; Fukuda, R.; Hasegawa, J.; Ishida, M.; Nakajima, T.; Honda, Y.; Kitao, O.; Nakai, H.; Vreven, T.; Throssell, K.; Montgomery Jr., J. A.; Peralta, J. E.; Ogliaro, F.; Bearpark, M. J.; Heyd, J. J.; Brothers, E. N.; Kudin, K. N.; Staroverov, V. N.; Keith, T. A.; Kobayashi, R.; Normand, J.; Raghavachari, K.; Rendell, A. P.; Burant, J. C.; Iyengar, S. S.; Tomasi, J.; Cossi, M.; Millam, J. M.; Klene, M.; Adamo, C.; Cammi, R.; Ochterski, J. W.; Martin, R. L.; Morokuma, K.; Farkas, O.; Foresman, J. B.; Fox, D. J. Gaussian 16 Rev. A.03, Wallingford, CT, 2016.

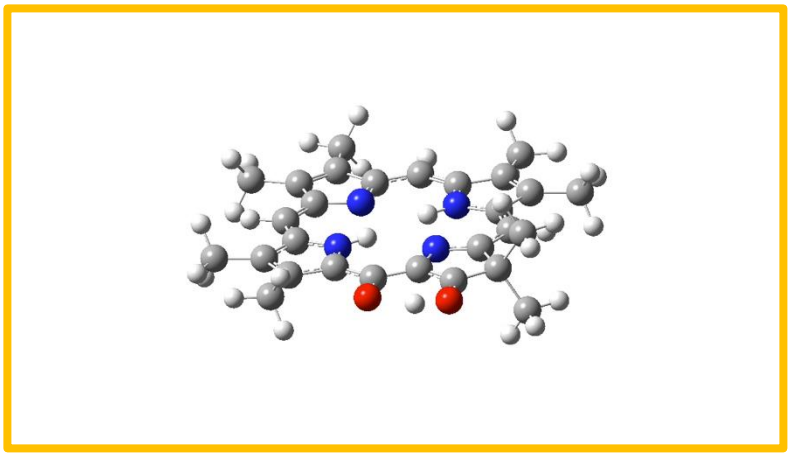

(mp4 – click to play)

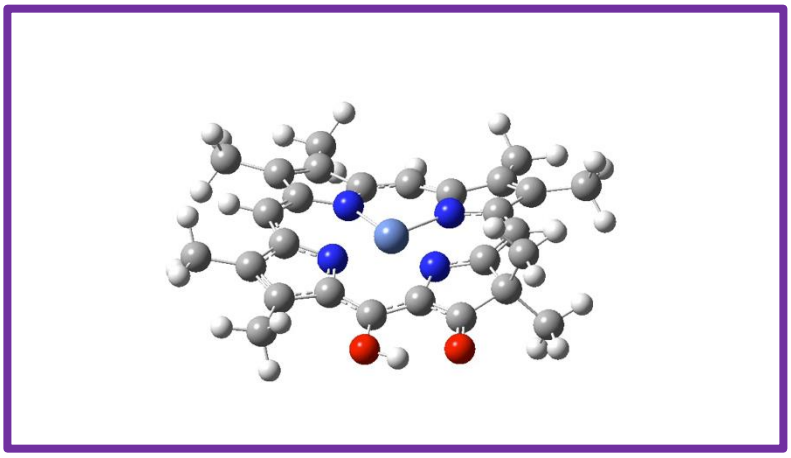

(mp4 – click to play)

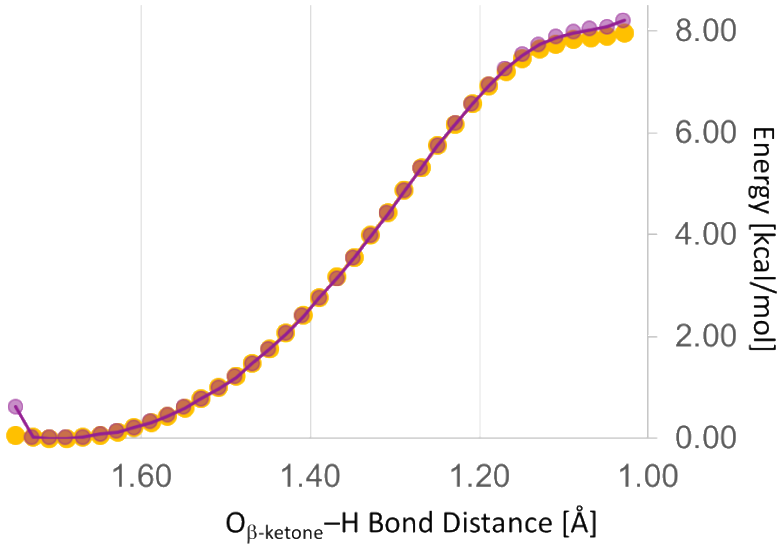

Figure S22. Computed energy trajectory for **9** (yellow) and **9Ni** (purple) moving the hydrogen atom from being bound to *meso*-oxygen (long $O_{\beta\text{-ketone}}$–H bond distance) the β-ketone oxygen (short $O_{\beta\text{-ketone}}$–H bond distance), showing the ~8 kcal/mol preference for the proton to be bound to the *meso*-oxygen atom. Clicking on the molecular models shows a movie of this trajectory.

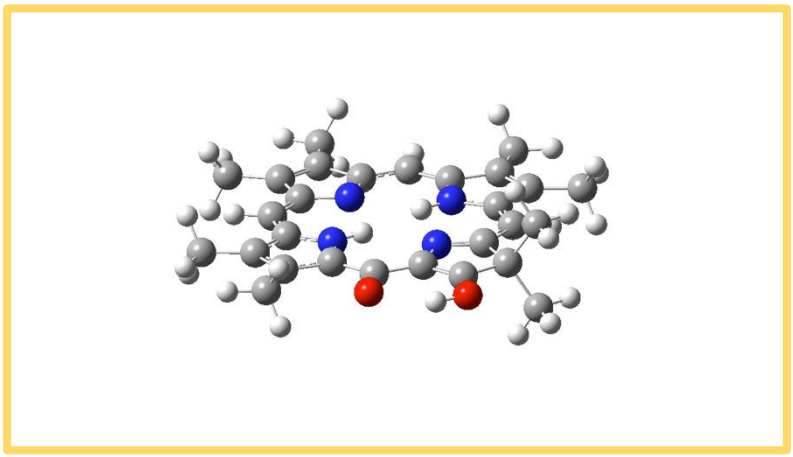

(mp4 – click to play)

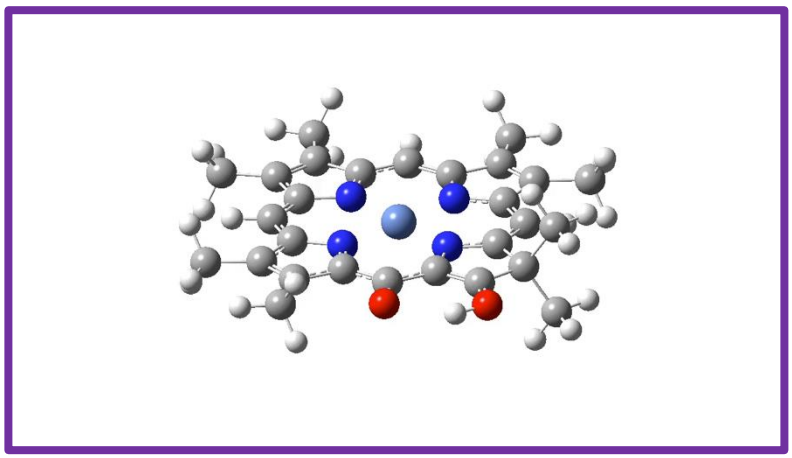

(mp4 – click to play)

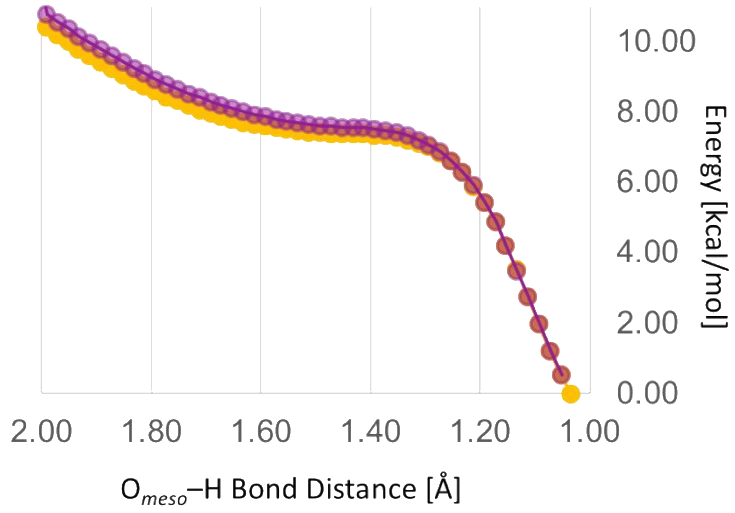

Figure S23. Computed energy trajectory for **9** (yellow) and **9Ni** (purple) moving the hydrogen atom from being bound to the β-ketone oxygen (long O_{meso}–H bond distance) to being bound to the *meso*-oxygen (short O_{meso}–H bond distance), showing the ~10 kcal/mol preference for the proton to be bound to the *meso*-oxygen atom. Clicking on the molecular models shows a movie of this trajectory.

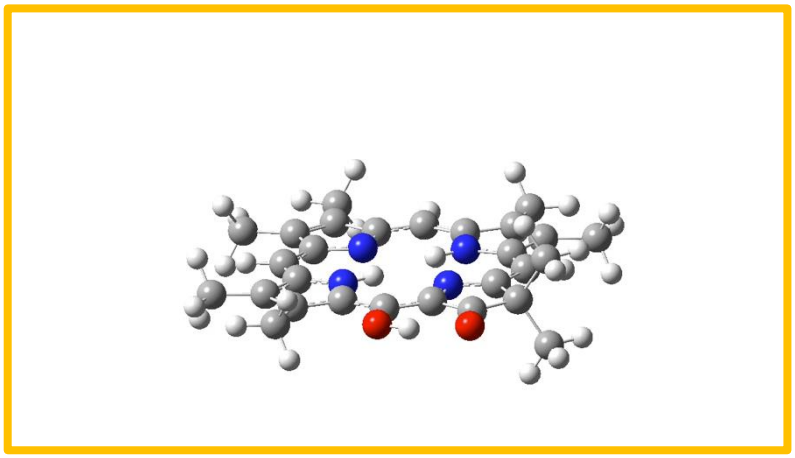

(mp4 – click to play)

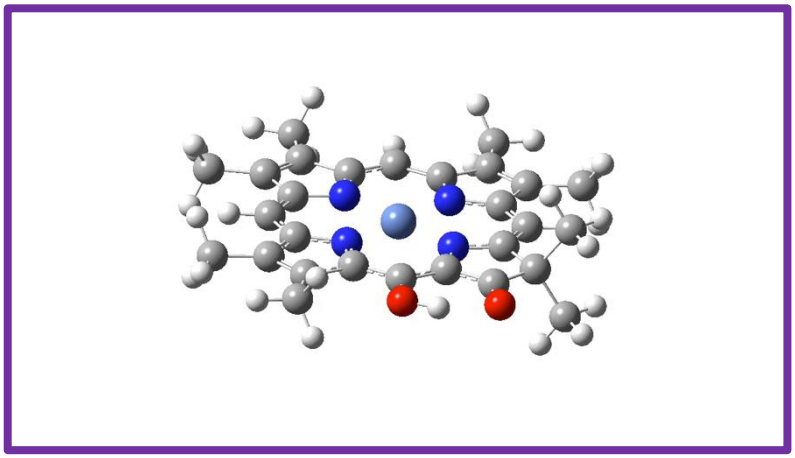

(mp4 – click to play)

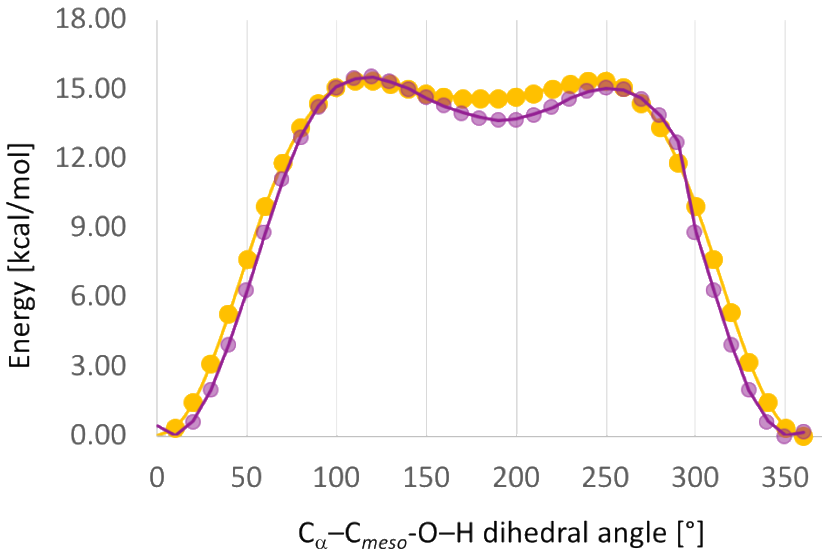

Figure S24. Skip-rope-like trajectory for **9** (yellow) and **9Ni** (purple) of the energy induced by hydroxyl group rotation, showing the absolute minima at the position of closest H-bond distance to the ketone oxygen. Clicking on the molecular models shows a movie of this trajectory.

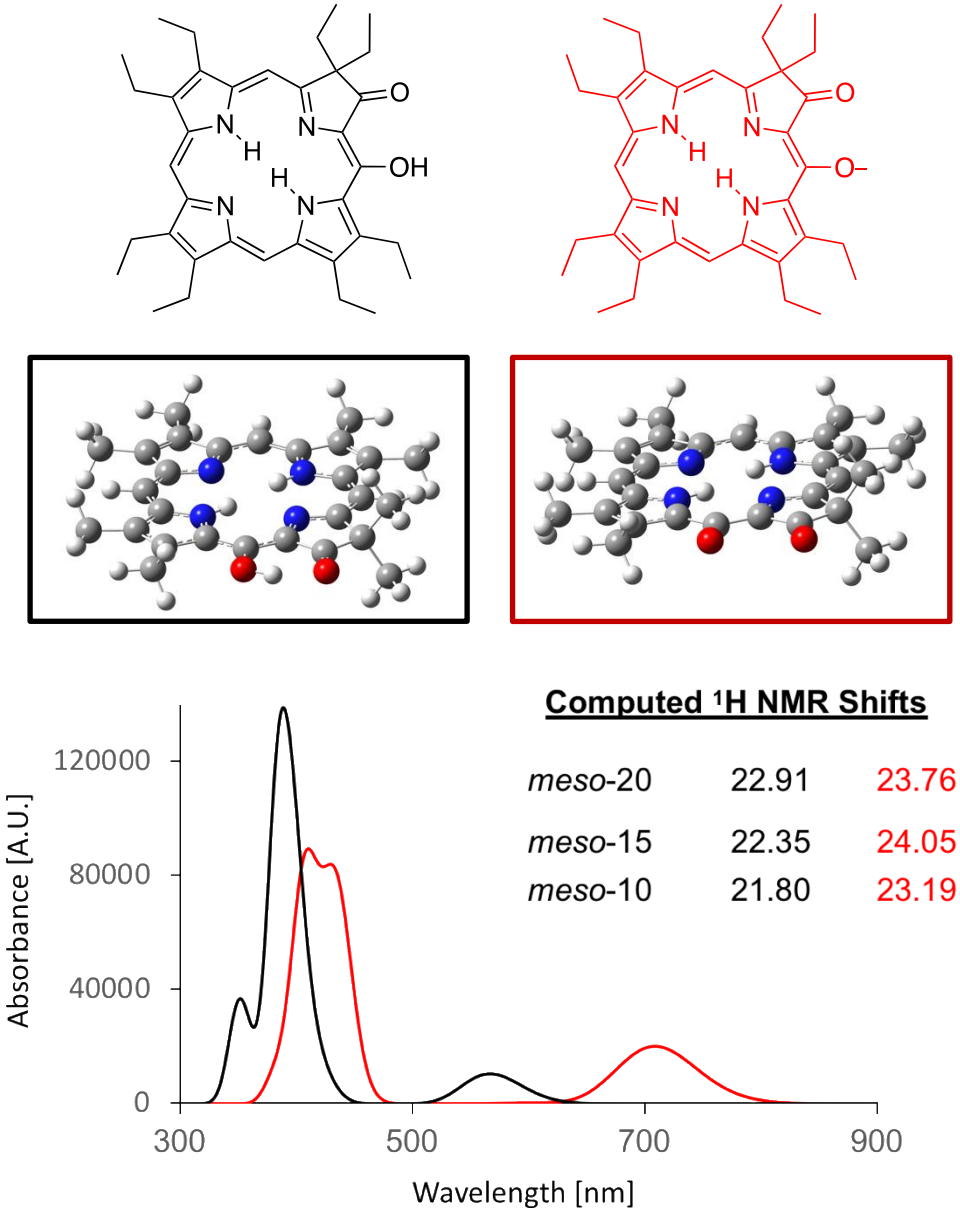

Figure S25. Computed optical spectra and ^{1}H NMR shifts of **9** in its neutral, *meso*-OH tautomeric form (black) and its anionic form carrying the charge on the *meso*–oxygen atom (red).

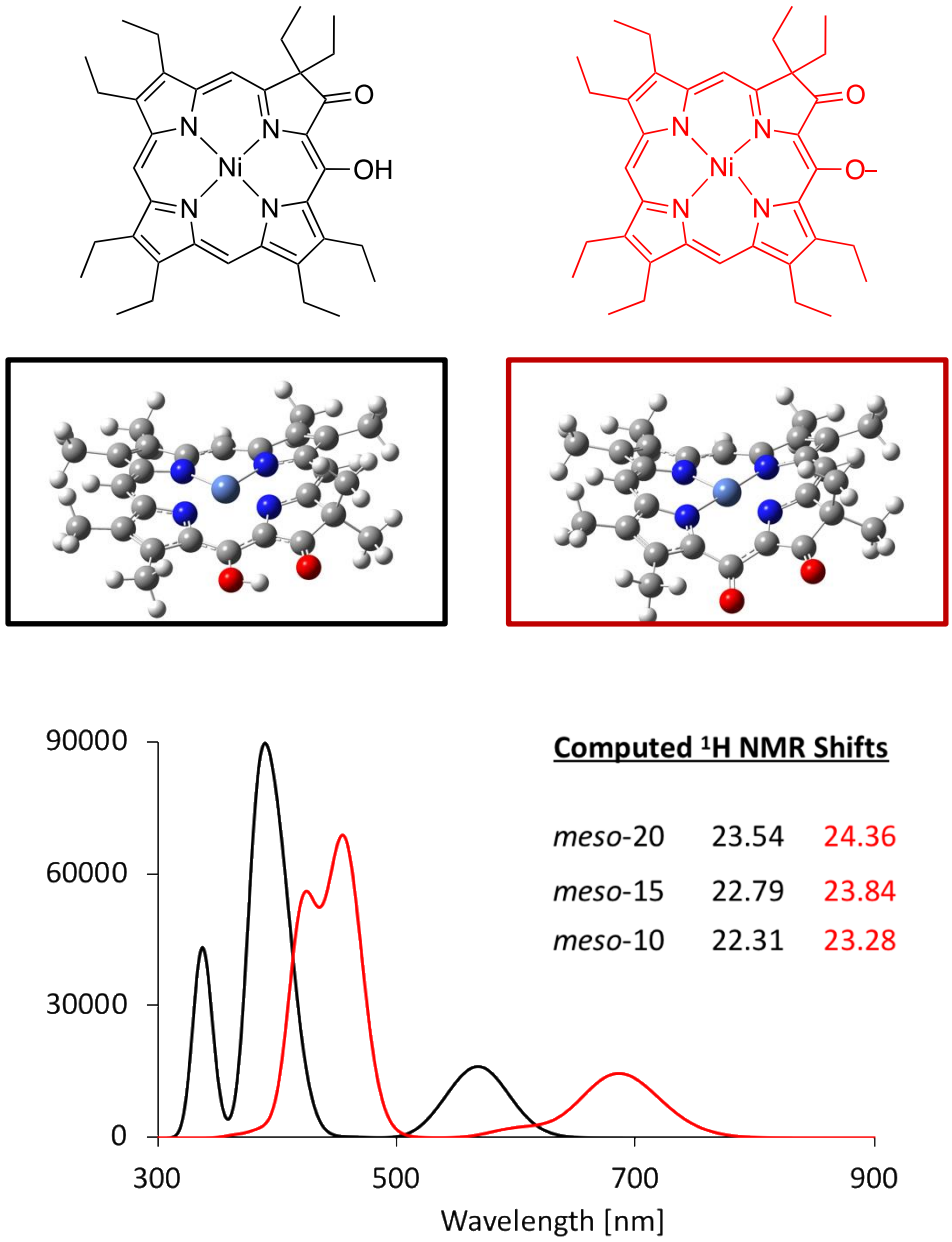

Figure S26. Computed optical spectra and ^{1}H NMR shifts of **9Ni** in its neutral, *meso*-OH tautomeric form (black) and its anionic form carrying the charge on the *meso*–oxygen atom (red).

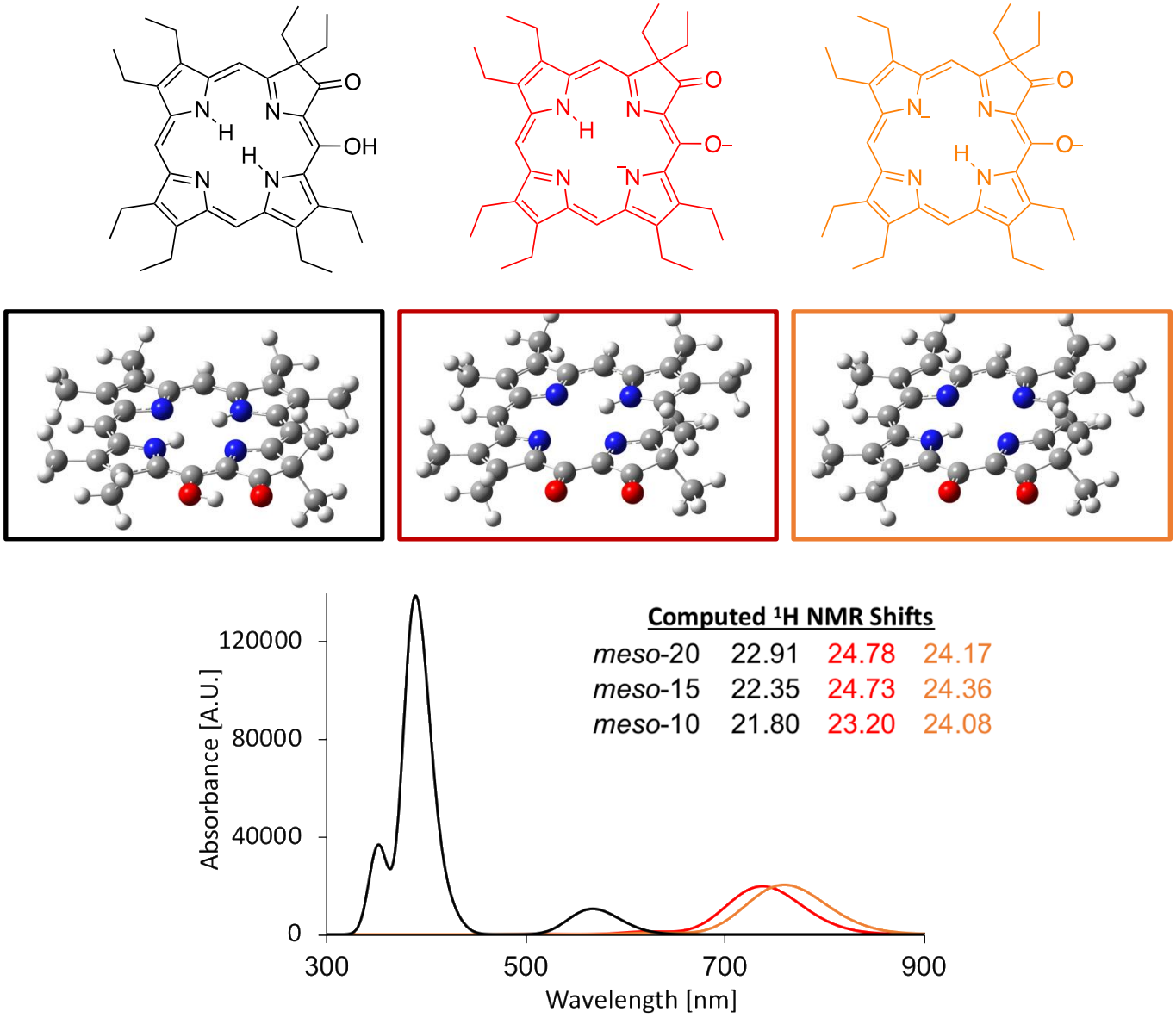

Figure S27. Computed optical spectra and ^{1}H NMR shifts of free base **9** in its neutral, *meso*-OH tautomeric form (black), and two dianionic forms carrying the charge on the *meso*–oxygen atom and either possible inner nitrogen indicated (red and orange).

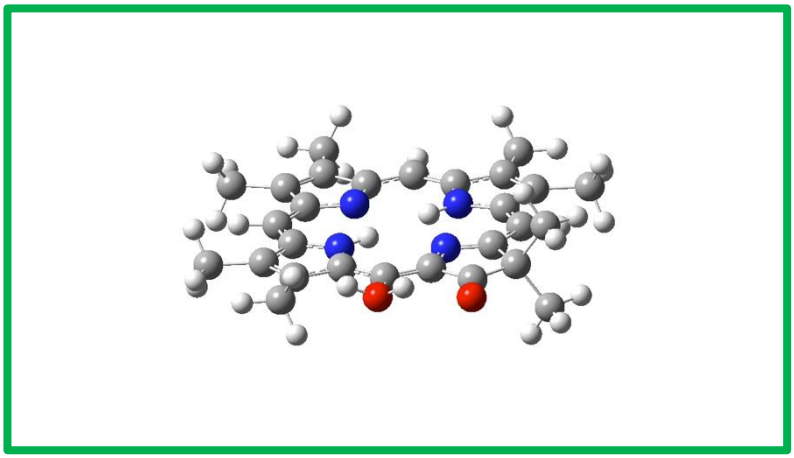

(mp4 – click to play)

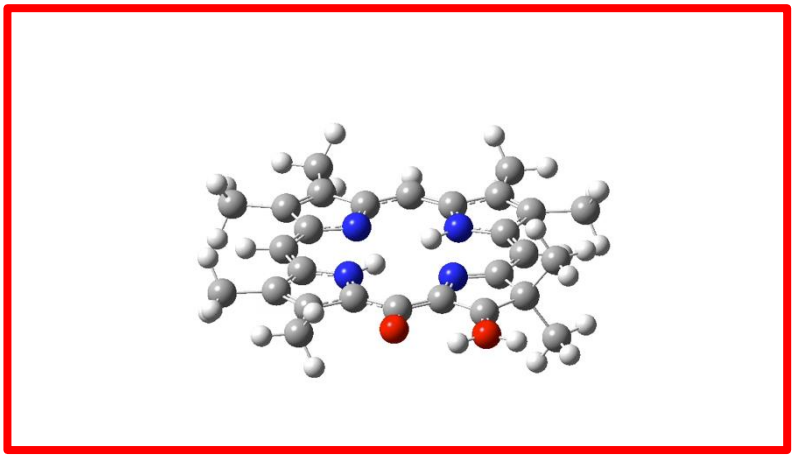

(mp4 – click to play)

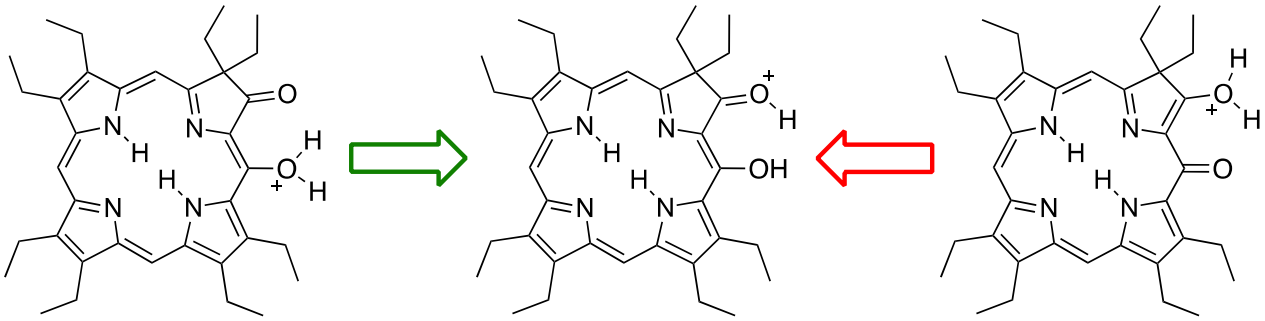

Figure S28. Computations of the mono-protonated form carrying both hydrogen atoms on either oxygen converge on a species in which either oxygen carries a single hydrogen, with the charge located on the pyrrolinone oxygen. Clicking on the molecular models shows a movie of the two trajectories.

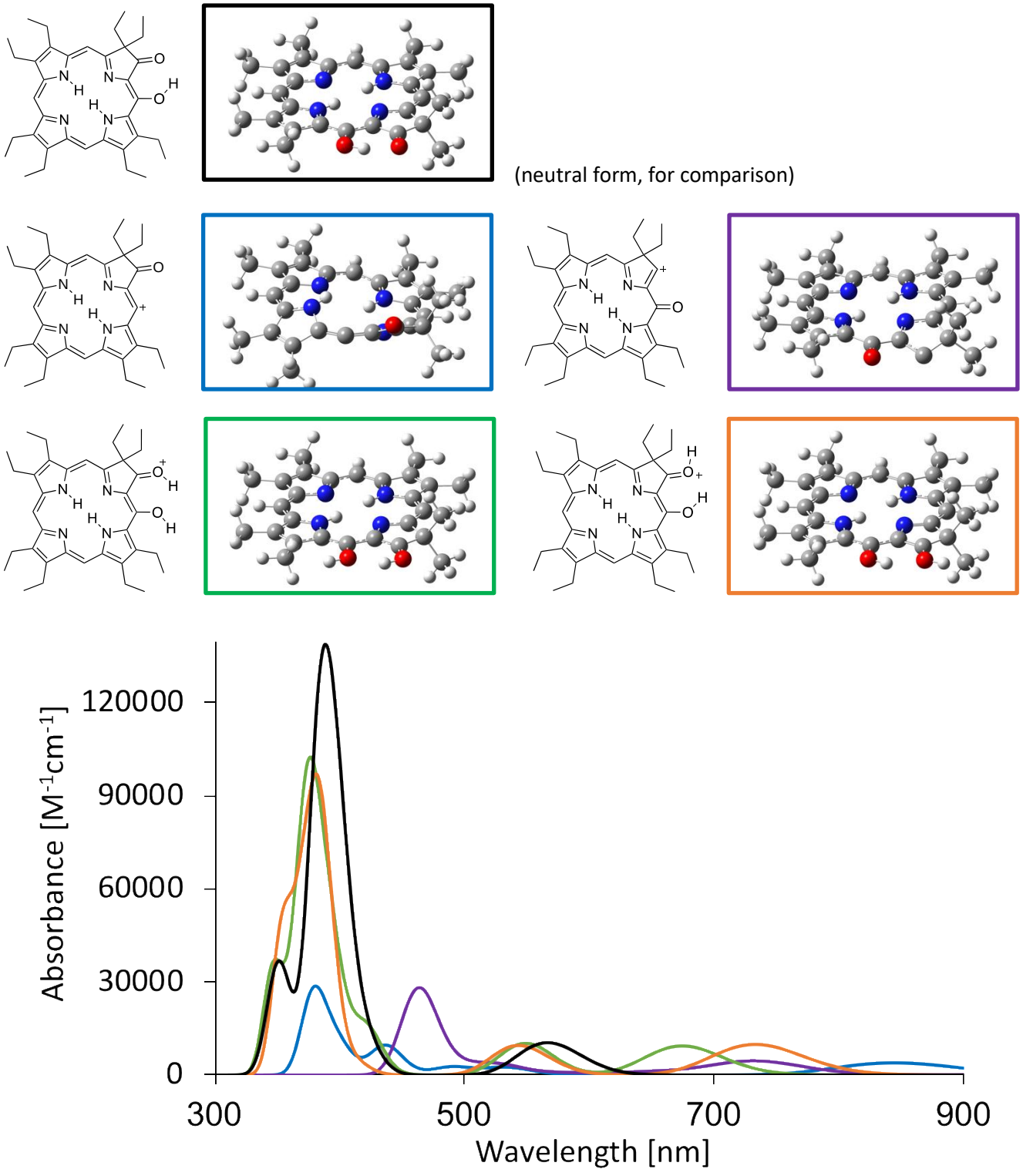

Figure S29. Computations of the UV-vis spectra of the various mono-protonated forms of **9** shown, in comparison to the neutral form of **9**.

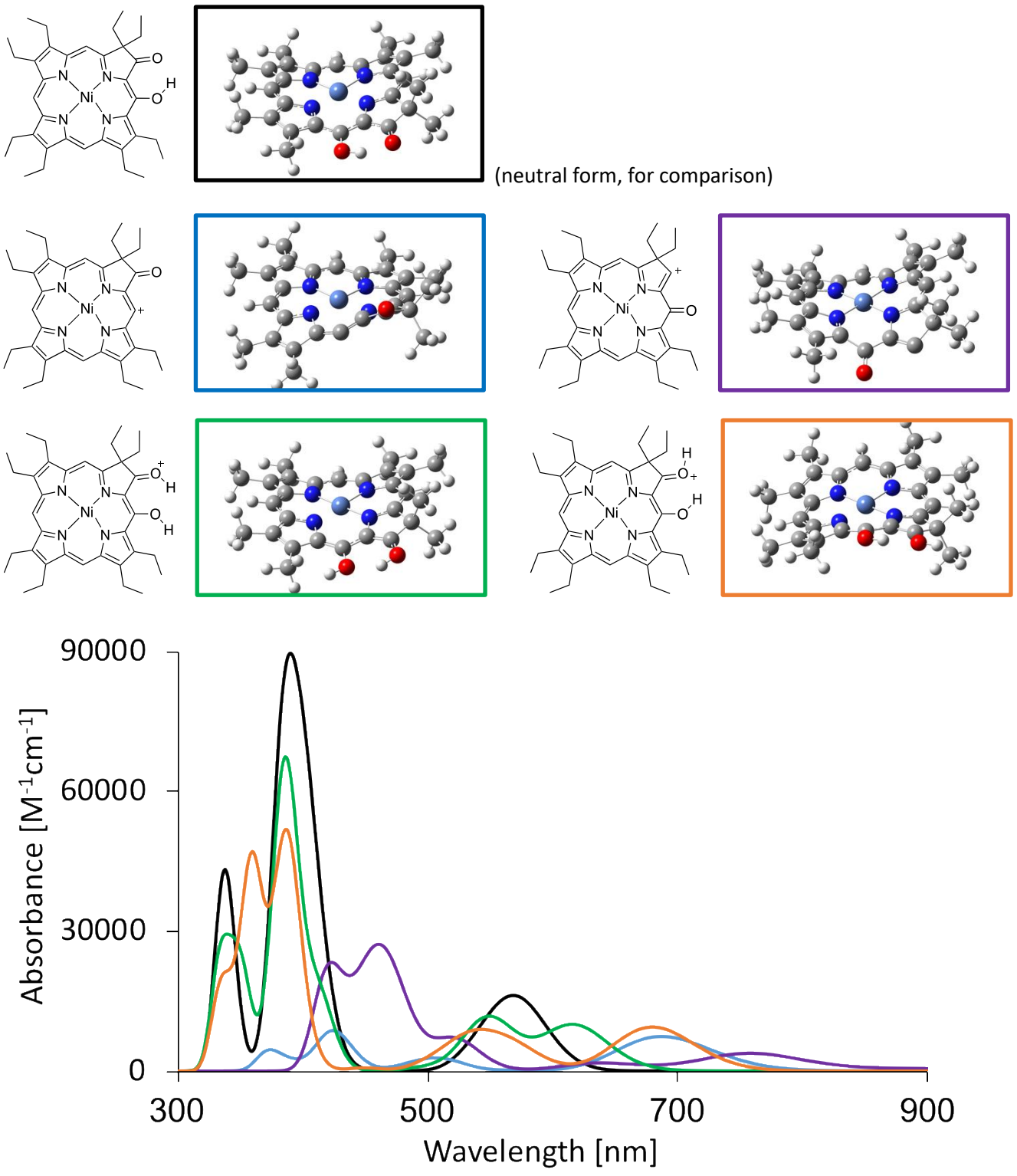

Figure S30. Computations of the UV-vis spectra of the various mono-protonated forms of **9Ni** shown, in comparison to the neutral form of **9Ni**.

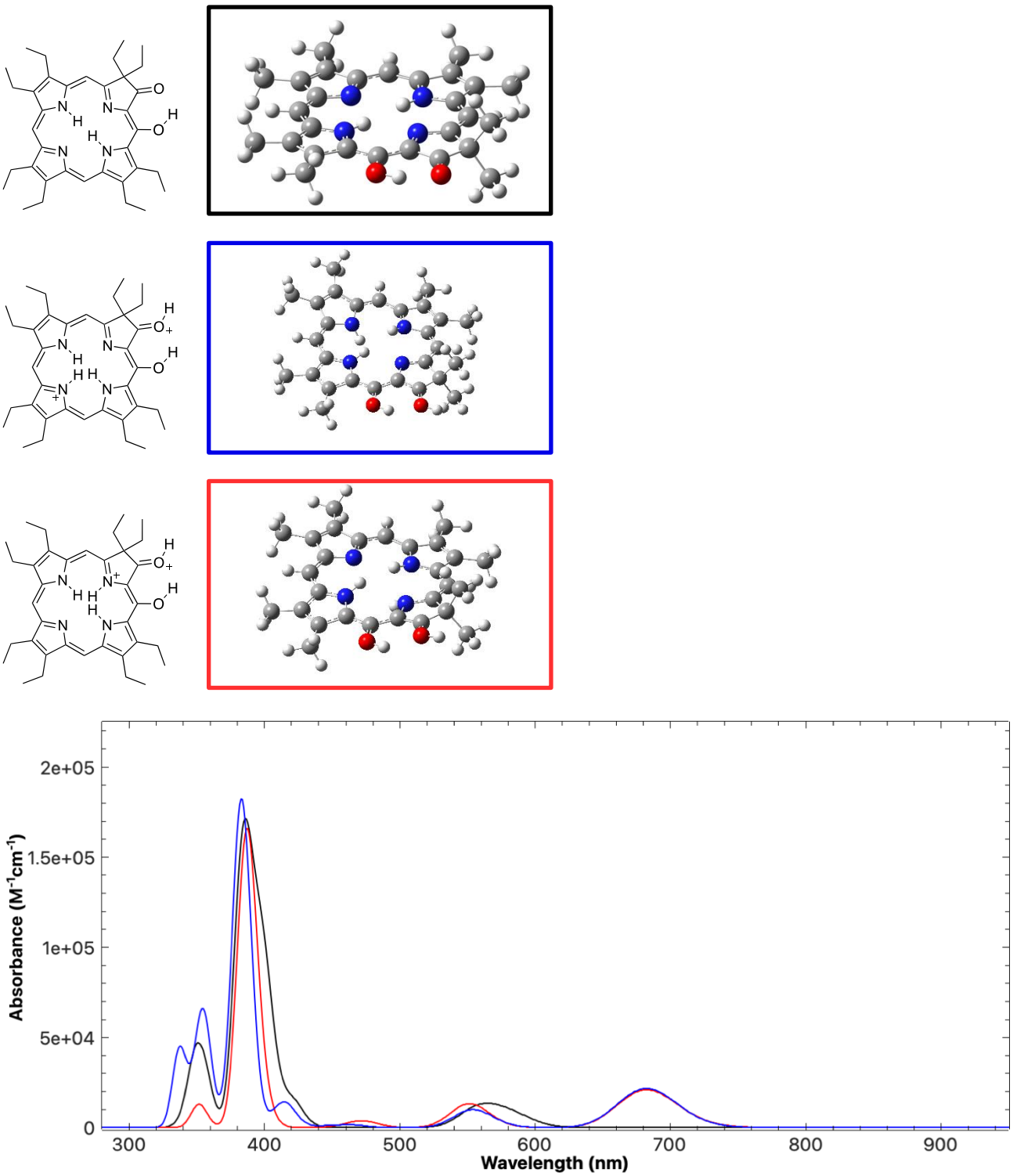

Figure S31. Computations of the UV-vis spectra of the di-protonated forms of **9** shown (in comparison to neutral form **9**).

Details to the X-ray diffractometry studies

Crystals of **9Ni** or **10** were mounted on a Mitegen micromesh mount in a random orientation and data were collected from a shock-cooled single crystals at 150(2) K on a Bruker AXS D8 Quest four circle diffractometer with an I-mu-S microsource X-ray tube using a laterally graded multilayer (Goebel) mirror as monochromator and a PhotonIII_C14 charge-integrating and photon counting pixel array detector. The diffractometer used CuK_α radiation (λ = 1.54178 Å). All data were integrated with SAINT V8.40B and a multi-scan absorption correction using SADABS 2016/2 was applied.[10] The structures were solved by dual methods with SHELXT and refined by full-matrix least-squares methods against F^2 using SHELXL-2019/2.[3,4]11 All non-hydrogen atoms were refined with anisotropic displacement parameters. Carbon bound hydrogen atoms, alcohol hydroxyl H atoms and H atoms of planar (sp^2 hybridized) N-H groups were refined isotropically on calculated positions using a riding model. Methyl CH_3 and hydroxyl H atoms were allowed to rotate but not to tip to best fit the experimental electron density. For water H atoms in **9Ni**, see below. U_{iso} values were constrained to 1.5 times the U_{eq} of their pivot atoms for methyl and hydroxyl groups and 1.2 times for all other hydrogen atoms.

Additional data collection and refinement details, including description of disorder (where present) can be found below. Complete crystallographic data, in CIF format, have been deposited with the Cambridge Crystallographic Data Centre. CCDC 2340919-2340920 contain the supplementary crystallographic data for this paper. These data can be obtained free of charge from The Cambridge Crystallographic Data Centre via www.ccdc.cam.ac.uk/data_request/cif.

In **9Ni**, one of the two independent molecules is disordered around an inversion center. The Ni metal atom is slightly offset from the center, resulting in 1:1 disorder for all atoms. The disordered moiety was restrained to have a similar geometry as the other not disordered molecule. For one of the ethyl groups, additional disorder was refined. The minor moiety was again restrained to have a similar geometry as the equivalent segment of the other not disordered molecule. The pyrrole sections and

[10] (a) Bruker, *SAINT*, *V8.40A*, Bruker AXS Inc., Madison, Wisconsin, USA. (b) L. Krause, R. Herbst-Irmer, G. M. Sheldrick, D. Stalke, *J. Appl. Cryst.* **2015**, *48*, 3–10, doi:10.1107/S1600576714022985.

[11] (a) G. M. Sheldrick, *Acta Cryst.* **2008**, *A64*, 112–122, doi:10.1107/S0108767307043930. (b) G. M. Sheldrick, *Acta Cryst.* **2015**, *C71*, 3–8, doi:10.1107/S2053229614024218.

adjacent atoms of the twice disordered segment were restrained to be close to planar. U_{ij} components of ADPs for disordered atoms closer to each other than 2.0 Å were restrained to be similar. Subject to these conditions the occupancy ratio for the twice disordered part refined to 0.313(8) to 0.187(8). A partially occupied water molecule is located in H-bonding distance to O1 of the not disordered molecule. It is in conflict with some of the disordered segments and its occupancy was freely refined. It's ADP was constrained to be the same as that of O1 of the not disordered molecule (to avoid an unreasonably small ADP paired with an underestimated occupancy). Water H atom positions were initially refined and O-H and H...H distances were restrained to 0.84(2) and 1.36(2) Å, respectively, while a damping factor was applied. One of the H atom positions was further restrained based on hydrogen bonding considerations (to O1_1). In the final refinement cycles the H atom positions were set to ride on their carrier oxygen atom and the damping factor was removed. Subject to these conditions the occupancy rate refined to 0.116(7).

In **10**, 1.5 molecules constitute the asymmetric content of the cell, with one molecule in a general position, and another one located atop an inversion center. The two molecules are related by a pseudo-translation. Slight modulation of atom positions, by up to 0.5 Å, breaks the symmetry required for the smaller cell. Both molecules exhibit disorder of a single hydroxyl group over the two possible positions with a hydrogen atom. For the molecule with inversion symmetry the disorder is exactly 1:1. For the other molecule the disorder refined to 0.496(2) to 0.504(2).

Structure Table

	9Ni	**10**
CCDC number	2340919	2340920
Empirical formula	$C_{36}H_{44.15}N_4NiO_{2.08}$	$C_{36}H_{46}N_4O_3$
Formula weight	624.85	582.77
Temperature [K]	150(2)	150(2)
Crystal system	triclinic	triclinic
Space group (number)	$P\overline{1}$ (2)	$P\overline{1}$ (2)
a [Å]	8.6985(10)	9.9024(9)
b [Å]	14.5755(16)	14.8290(14)
c [Å]	20.098(2)	17.1682(17)
α [°]	109.334(7)	77.175(4)
β [°]	97.626(8)	74.867(4)
γ [°]	91.299(7)	87.062(4)
Volume [Å^3]	2377.1(5)	2372.8(4)
Z	3	3
ρ_{calc} [gcm^{-3}]	1.309	1.223
μ [mm^{-1}]	1.180	0.616
F(000)	998.3	942
Crystal size [mm^3]	0.070×0.060×0.010	0.330×0.310×0.060
Crystal colour	green	purple
Crystal shape	flake	plate
Radiation	CuK_α (λ=1.54178 Å)	CuK_α (λ=1.54178 Å)
2Θ range [°]	4.71 to 162.32 (0.78 Å)	5.46 to 159.94 (0.78 Å)
Index ranges	-11 ≤ h ≤ 10 -18 ≤ k ≤ 18 -25 ≤ l ≤ 24	-12 ≤ h ≤ 12 -18 ≤ k ≤ 18 -21 ≤ l ≤ 21

Reflections collected	30684	74970
Independent reflections	9596 R_{int} = 0.1099 R_{sigma} = 0.1184	10228 R_{int} = 0.0658 R_{sigma} = 0.0419
Completeness	98.7 %	99.9 %
Data / Restraints / Parameters	9596/743/891	10228/0/611
Goodness-of-fit on F^2	1.009	1.073
Final *R* indexes [$I \geq 2\sigma(I)$]	R_1 = 0.0732 wR_2 = 0.1853	R_1 = 0.0473 wR_2 = 0.1354
Final *R* indexes [all data]	R_1 = 0.1344 wR_2 = 0.2363	R_1 = 0.0557 wR_2 = 0.1431
Largest peak/hole [eÅ^{-3}]	0.69/-0.54	0.35/-0.22
Extinction coefficient	0.0027(4)	

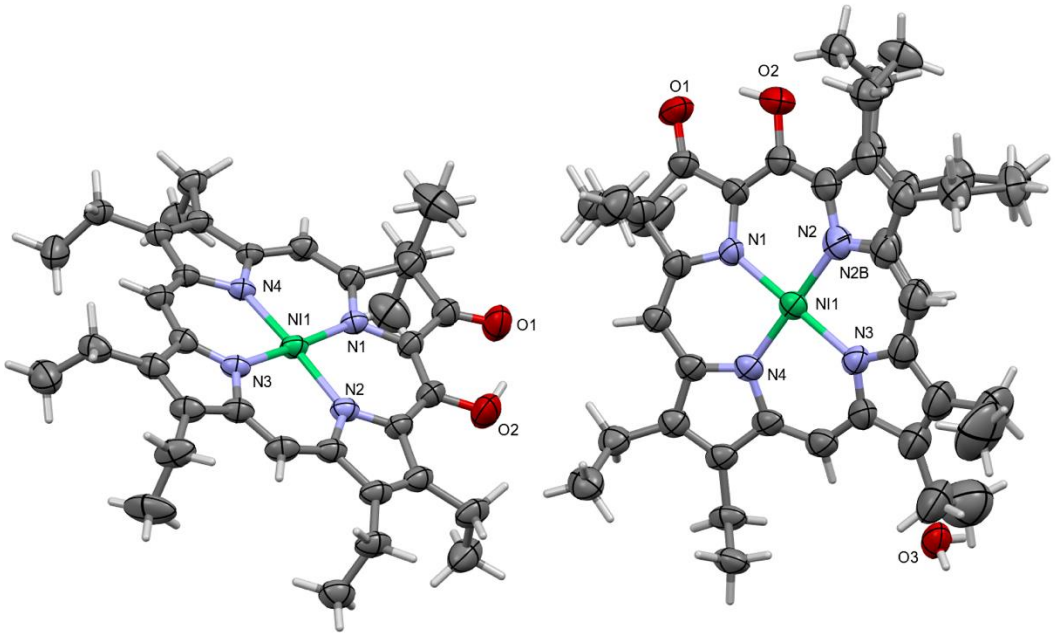

Figure S32. Thermal ellipsoid representation for compound **9Ni**, at 50% probability levels showing molecule 1 (left) and 2 (right) and the partially occupied water molecule. Disorder by inversion for molecule 2, moiety numbers and C and H labels omitted for clarity.

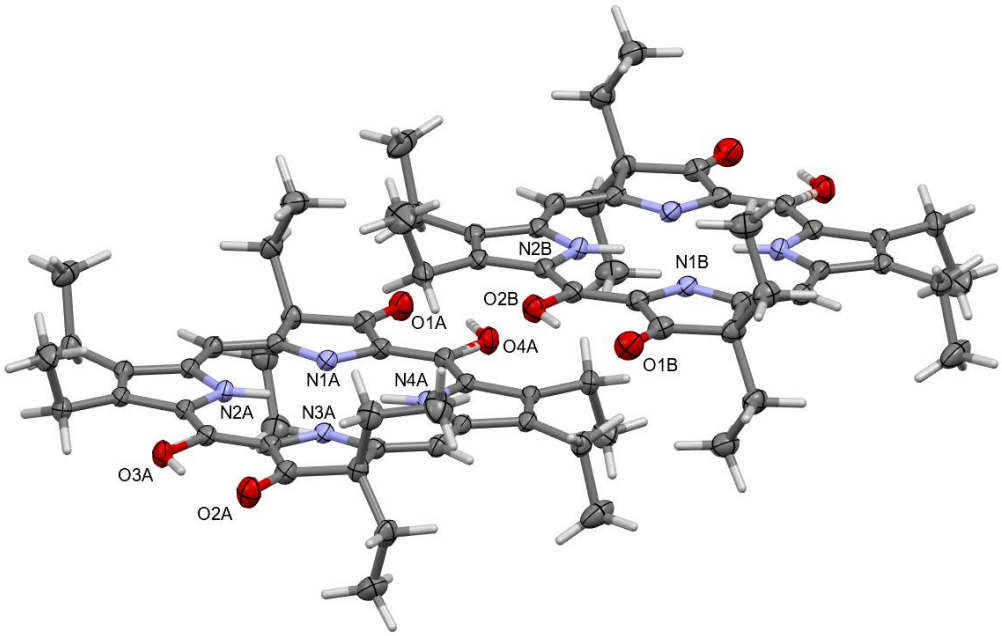

Figure S33. Thermal ellipsoid representation for compound **10**, at 50% probability levels. C and H labels and those for symmetry created atom (molecule B) omitted for clarity.